Finite element methods for finding the complex Floquet propagation constant of three dimensional periodic structures

Ali Bostani

Department of Electrical & Computer Engineering

McGill University

Montreal, Canada

May 2012

A thesis submitted to McGill University in partial fulfillment of the requirements of the degree of PhD in Electrical Engineering.

Abstract

Periodic structures have been widely used in the radio frequency (RF) and microwave industries in the past few decades. Understanding the modal behavior of these structures requires an eigenvalue study called dispersion analysis, to which the finite element method (FEM) has been successfully applied. The classical FEM approach is to specify a purely imaginary propagation constant and find the corresponding frequency. This method provides information regarding the behavior in the passband, but not in the stopband, and moreover cannot accommodate lossy or frequency-dependent materials.

Recently a new FEM was reported that allows the user to specify the frequency and find the complex propagation constant. However, the method is computationally inefficient and unable to handle realistic 3D problems. The focus of this thesis is on improving the efficiency, in three steps. In the first step, the quadratic matrix eigenvalue problem is turned into a linear eigenproblem of the same size without loss of generality and a sparse method is used to solve it. This reduces the computational cost from $\boldsymbol{O(n^3)}$ to $\boldsymbol{O(n^{1.6})}$, where $\boldsymbol{n}$ is the matrix dimension. With this dramatic improvement, the method is able to analyze realistic 3D geometries for the first time. In the second step, a model order reduction (MOR) technique is applied. With MOR, only two full-size eigenproblems need to be solved, at a single"expansion point" frequency, in order to generate the dispersion diagram over a range of frequencies. Since the full-size analysis does not need to be repeated at a large number of frequency points, the overall computational cost is lowered considerably. Despite the efficiency of this approach, it suffers from a limited bandwidth because the error increases as the frequency moves further from the expansion point. In the third step, an adaptive algorithm is developed which uses multiple expansion points and a smart error estimator which indicates where a new expansion point needs to be employed so that the error does not exceed a given threshold. Also, an adaptive mode tracking system is developed which adjusts the frequency step size to guarantee that the same propagation mode is being tracked over the whole frequency range.

At each step, the new methods are applied to four periodic structures: a triply periodic array of metallic cubes and three planar structures used for noise suppression in high-speed digital circuits. In addition, the adaptive method is applied to a singly-periodic iris-loaded waveguide. The computational cost for these cases is at least an order of magnitude lower than even the cost of solving the full size linear eigenvalue problem at each frequency.

Résumé

Dans les dernières décennies Les structures périodiques ont connu un très grand succès dans les domaines technologiques comme la radiofréquence (RF) et les micro- ondes suite à une large utilisation.

La compréhension du comportement modal de ces structures nécessite une étude des valeurs propres appelée analyse de la dispersion, à laquelle la méthode des éléments finis (FEM) a été appliquée avec succès. L'approche classique consiste à spécifier une constante de propagation purement imaginaire et de trouver la fréquence correspondante. Cette méthode fournit des informations concernant le comportement dans la bande passante, mais pas dans la bande d'arrêt, et en outre ne permet pas d'appliquer des matériaux avec pertes ou qui dépendent de la fréquence.

Récemment, une nouvelle variante de la FEM a été rapportée et qui permet à l'utilisateur de spécifier la fréquence et de trouver la constante de propagation complexe. Cependant, la méthode est arithmétiquement inefficace et incapable de gérer les problèmes réels en 3D.

L'objectif de cette thèse porte sur l'amélioration de l'efficacité, en trois étapes.

Dans la première étape, le problème de la forme quadratique de matrice à valeurs propres est transformé en un problème linéaire qui a la même taille de la matrice sans perte de généralité, une méthode pour matrices creuses a été utilisée pour le résoudre. Ce qui a permis de réduire le coût du calcul de $O(n^3)$ à $O(n^{1.6})$, où n est la dimension de la matrice.

Grâce à cette amélioration spectaculaire, la méthode est capable d'analyser les géométries réalistes 3D pour la première fois.

Dans la deuxième étape, une technique de réduction d'ordre du modèle (MOR) est appliquée. Avec MOR, à un seul «point d'expansion» fréquentiel, seulement deux solutions complètes de valeurs propres doivent être obtenues afin de générer le diagramme de dispersion sur toute une bande de fréquences. Puisqu'il n'est plus

nécessaire de refaire une résolution complète du système en entier à chaque point de fréquence, le coût global de calcul est considérablement réduit. Malgré l'efficacité de cette approche, la méthode souffre d'une bande de convergence réduite, car l'erreur augmente au fur et à mesure que la fréquence s'éloigne du point d'expansion.

Dans la troisième étape, un algorithme adaptatif a été développé. Cet algorithme utilise des points d'extension multiples et un estimateur d'erreur intelligent qui nous indique l'endroit où on doit utiliser un autre point d'expansion de telle sorte que l'erreur ne dépasse pas un seuil donné. De plus, un système de suivi adaptatif a été élaboré, qui ajuste la valeur du pas fréquentiel pour garantir que le même mode de propagation est suivi sur toute la bande de fréquence.

A chaque étape, les nouvelles méthodes ont été appliquées pour quatre structures périodiques: un tableau triplement périodique de cubes métalliques et trois structures planaires utilisées pour la suppression du bruit dans les circuits numériques à grande vitesse. En outre, la méthode adaptative a été appliquée à un guide d'ondes à période unique chargé d'iris. Le coût de calcul pour ces cas est d'au moins un ordre de grandeur plus faible que le même coût de la résolution de la taille linéaire du problème au complet aux valeurs propres et à chaque fréquence.

Acknowledgement

I would like to express my deepest respect and most sincere gratitude to my supervisor, Professor Jon Webb, for his guidance and encouragement at all stages of my work. His wide knowledge in electromagnetics, finite element method and linear algebra and his logical and smart way of thinking have been of great value for me. I cannot even start to thank him enough for his patience and kindness. I am greatly indebted to his understanding, encouraging and professional attitude which have provided an excellent basis for the present thesis. I always tell my friends that if I could, I would never finish my PhD, as it has been literally the best period of my life.

I owe my loving thanks to my wife Sara who has lost a lot due to my research abroad. Without her encouragement and understanding it would have been impossible for me to finish this work. My special gratitude is due to my parents, my brothers (Hassan and Mohammad Hossein) and my sister (Fatemeh) for their loving support.

Table of Contents

List of Figures

Chapter 1

Introduction

People have always been interested in periodicity. There are many examples of periodic structures in nature. For example, bees create their hives in a periodic way (Fig. 1.1).

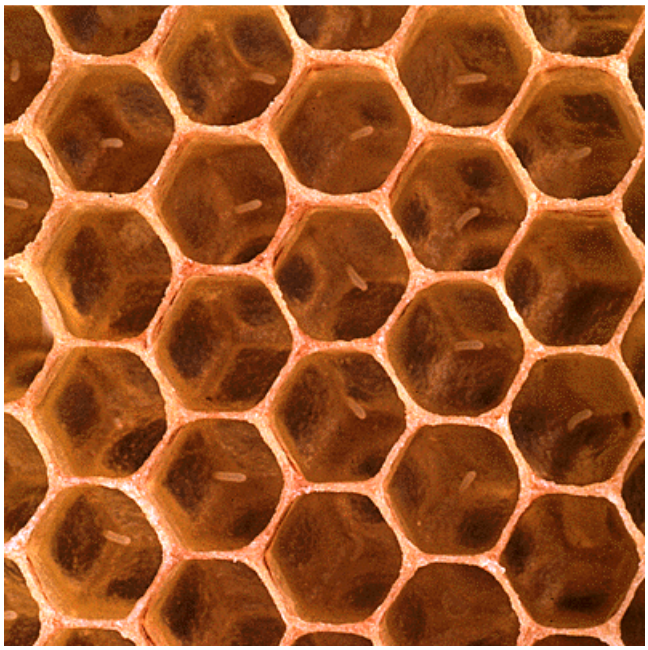

Fig. 1.1 The periodic pattern of a bee hive. (Taken from [36]).

The existence of different seasons in a year is also a periodic phenomenon. Observing periodic structures in nature encouraged people to think of using this concept artificially to obtain some new and extraordinary properties. Many periodic structures have been proposed and used in different branches of engineering.

In scientific terms, a periodic structure is defined as a structure in which a single region of space containing a specific arrangement of materials is repeated over and over again, indefinitely. The single region which is repeated is called the *unit cell*. An example is shown in Fig. 1.2. The unit cells can be of different, e.g., hexagonal (Fig. 1.1) or cubic (Fig. 1.2).

A periodic structure can be singly, doubly or triply periodic. A singly periodic structure is a structure in which the unit cell is repated only in one direction. The unit cell in doubly and triply periodic structures is repeated in two or three directions respectively. Figs. 1.1 and 1.2 are both examples of triply periodic structures.

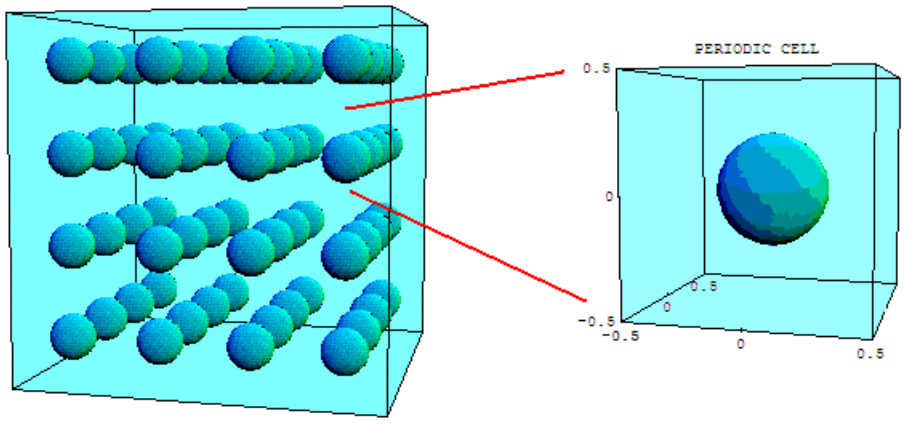

Fig. 1.2 A periodic structure and one unit cell of the structure [37].

Periodic structures are widely used in radio-frequency (RF) and microwave engineering because of their ability to create passbands and stopbands. The passband is a range of frequencies over which the structure allows electromagnetic waves to propagate. On the other hand the stopband is a range of frequencies over which the structure blocks electromagnetic waves. The first question that arises when designing a microwave system including a periodic structure is the exact location of the passbands and stopbands. The second question is the level of the attenuation in the stopband and the phase constant of the wave in the passband.

Analyzing periodic structures in order to calculate the propagation constant as a function of frequency is called dispersion analysis. Dispersion analysis not only locates the passbands and stopbands, but also gives us the phase constant in the passband and the attenuation constant in the stopband.

The beauty of the dispersion analysis of periodic structures lies in the fact that we do not need to model the whole structure to be able to analyze it. We only need to model the unit cell.

There are several different ways to analyze the unit cell. The classical method of dispersion analysis is transmission line modelling. As the name suggests, in this method the unit cell is modeled with lengths of transmission line and lumped components. The important advantage of this kind of modelling is the rapidness of the method. On the other hand the disadvantage is poor accuracy, because of a circuit level approximation of Maxwell's equations. Also the method is not able to handle unit cells with complicated geometries.

The other way to perform dispersion analysis is to use a numerical method like the finite element method or the boundary element method. In this thesis, the finite element method is used.

The Finite Element Method (FEM) is used widely in engineering because of its accuracy and flexibility in handling very complicated geometries. FEM is based on dividing the structure into a number of small elements, approximating the field

in each element and then assembling the elements to obtain a matrix equation. Solving the matrix equations gives the field.

The following section reviews the different methods for analyzing periodic structures and obtaining propagation constants.

1.1 Literature review

Methods for the dispersion analysis of periodic structures can be classified into two major categories: methods which model the unit cell with transmission lines and lumped components and methods based on numerical analysis of the electromagnetic field in the unit cell, such as FEM. From now on the second category will be called field analysis methods.

After a brief review of Floquet's theorem there will be survey of the literature in the two main categories.

1.1.1 Floquet's theorem

In 1883 Floquet managed to solve the differential equation of the form

$$\frac{dF}{dz} = f(z)F \tag{1.1}$$

where $f(z)$ is a known periodic function and F is an unknown function of z [1]. He transformed the periodic system into a linear system by giving a canonical form to the matrix solutions of the system [1]. Floquet's theorem was the mathematical basis for the application of the periodic boundaries in solid state physics which was proposed in 1928 by Bloch [2].

In 1966 Collin discussed Bloch waves in singly-periodic microwave structures [3]. He showed that a time harmonic electromagnetic field at any point in one cell is $e^{-\gamma D}$ times the field at the corresponding point in the preceding cell, where D is the cell length and $\gamma = \alpha + j\beta$ is a complex propagation constant, called the Floquet constant, which is not a function of position within the cell. Naturally γ is a function of the frequency of oscillation, or, equivalently, the free-space wavenumber, k_0.

The proof of this result is as follows. According to Floquet's theorem, for a structure which is periodic in the z direction the complex vector field at an arbitrary point can be written as

$$\mathbf{F}(x, y, z) = e^{-\gamma z}\mathbf{F_p}\,(x, y, z) \tag{1.2}$$

where $\mathbf{F_p}\,(x, y, z)$ is a periodic function of z with period D. Now the field at point $z + D$, according to (2), would be:

$$\mathbf{F}(x, y, z + D) = e^{-\gamma(z+D)}\mathbf{F_p}\,(x, y, z + D) \tag{1.3}$$

and since $F_p(x, y, z)$ is a periodic function with period D,

$$\mathbf{F_p}\,(x, y, z + D) = \mathbf{F_p}\,(x, y, z) \tag{1.4}$$

Therefore

$$\begin{aligned}\mathbf{F}(x, y, z + D) &= e^{-\gamma(z+D)}\mathbf{F_p}\,(x, y, z) = e^{-\gamma D}e^{-\gamma z}\mathbf{F_p}\,(x, y, z) \\ &= e^{-\gamma D}\mathbf{F}(x, y, z)\end{aligned} \tag{1.5}$$

which is the desired result.

Looking at equations (1.2) to (1.5), we can see that two different approaches can be considered to find the electromagnetic field $\boldsymbol{F}$:

1) Find the spatial harmonics of the periodic function $F_p(x, y, z)$ and use equation (1.2) to get the field.

2) Find the field for one unit cell and use equation (1.5) to express the field all along the structure.

The first approach requires the expansion of $F_p(x, y, z)$ into a Fourier series. This way the electromagnetic field will be solved as:

$$\mathbf{F}(x, y, z) = \sum_n \mathbf{F}_{pn}(x, y)e^{-\gamma_n z} \tag{1.6}$$

where in this equation:

$$\gamma_n = \alpha + j(\beta + \frac{2n\pi}{D}) \tag{1.7}$$

$$\mathbf{F}_{pn}(x,y) = \frac{1}{D}\int_0^D \mathbf{F}_p(x,y,z)e^{j\frac{2n\pi}{D}z}\,dz \tag{1.8}$$

The Floquet mode number is defined as the phase constant of the n^{th} harmonic in (1.6). To find the complex mode numbers in (1.7) and Floquet vector fields in (1.8), the plane wave expansion method has been proposed [33]. This provides the solution for the complex Fourier coefficients only for singly periodic structures. For doubly and triply periodic problems there is no general solution for arbitrary geometries, only some formulas for simple geometries.

On the other hand the second approach, finding the field for a single unit cell and then applying equation (1.5), provides us with a finite domain and gives us the freedom to use different methods to find the field inside that domain. Finding the field inside the unit cell means that the field has been found everywhere in the structure.

The rest of this chapter explains the various methods reported in literature for the second approach. Both transmission-line modelling and field analysis methods will be reviewed.

1.1.2 Transmission line modelling of the unit cell

Modelling the unit cell of periodic structures by transmission line components is a inexpensive way to analyze simple geometries like periodically loaded waveguides [4].

In this method, wave propagation is formulated based on transmission line theory. To date, transmission line modelling has been applied to printed structures loaded with lumped elements [6], [7], microstrip periodic structures [8], [9], and some metamaterials [10], [11].

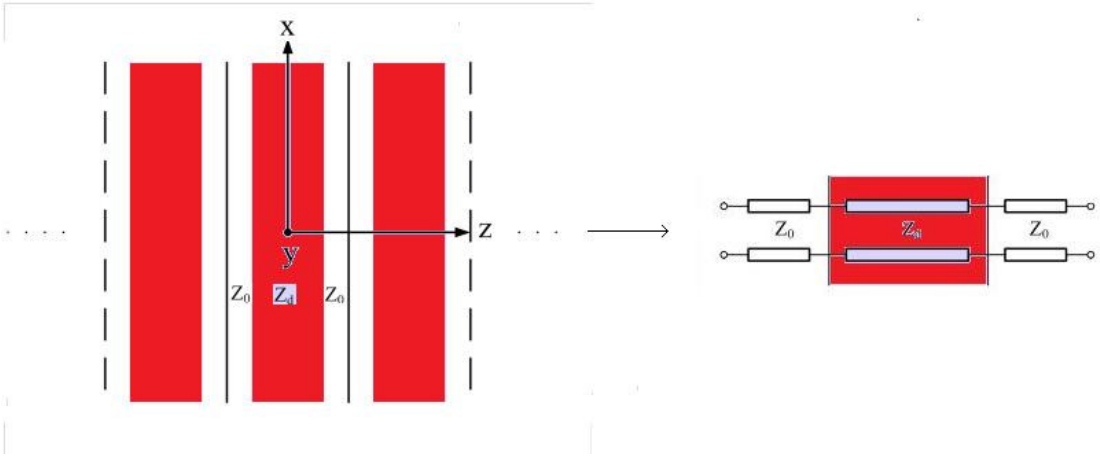

Fig. 1.3 A singly periodic structure and its transmission line model. The Z0 regions are free space and the red regions are dielectric slabs.

Fig. 1.3 shows a typical transmission line model for the one dimensional, singly-periodic structure shown on the left. As we can see in the picture, each part of the unit cell is modelled with a different length of transmission line. In this example the two short lines with characteristic impedance of Z_0 represent free space and the long line with characteristic impedance of Z_d represents the dielectric slab.

Instead of different lengths of transmission lines, the cell can also be modeled by capacitive and inductive lumped components.

Now, to characterize the propagation along the periodic structure, we only need to analyze the behaviour of the circuit parameters (voltage V and current I) of the transmission line model by multiplying the transfer matrix of the cascade composition of the three transmission line sections. That will give us an ABCD matrix [3] of the unit cell which relates the incoming (left-hand side) voltage and current to the outgoing (right-hand side) voltage and current. As the periodicity of the structure imposes another transfer matrix in terms of the propagation constant, equating the two ABCD matrices will give us the unknown propagation constant.

Doubly periodic structures can also be modeled with transmission line sections and lumped elements. The general idea is the same as before, but with this difference: unlike the singly periodic case, we deal with it as a multiple-input multiple-output system and we find the transfer matrix for any path between an input and an output. As an example in Figure 4, we would have four ABCD matrices which will give us four linear equations to figure out the dispersion parameters of the unit cell.

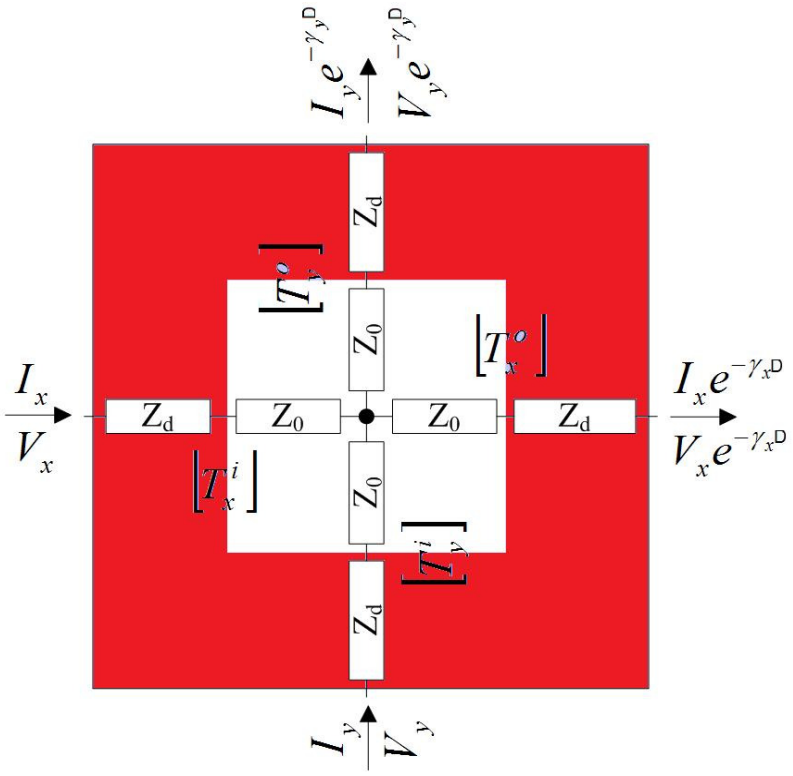

Fig. 1.4 A two dimensional doubly periodic structure

1.1.3 Field analysis methods

Computational electromagnetics has found a significant place in the design and analysis cycles of the microwave industry. Among the many computational methods, the following are reported in the literature for analyzing periodic structures [13]: the finite difference method in the time domain (FDTD) and in the frequency domain (FDFD), the method of moments (MoM), the finite element method (FEM), and the transmission line matrix method (TLM).

There are two completely different ways to employ any of these methods in periodic structure analysis. One way, which is called deterministic, is to examine

the fields inside a periodic structure in the presence of a known source, e.g., an incident plane wave.

The other way of analyzing periodic structures is dispersion analysis or eigen-analysis. This approach deals with the unit cell of the periodic structure as a source free object and finds the modes of this structure by solving an eigenvalue problem.

Since this thesis is concerned with dispersion analysis, the following survey will largely concentrate on methods for that kind of analysis.

1.1.3.1 Method of moments

MoM or the boundary element method (BEM) is a computational method for solving linear partial differential equations which have been formulated as integral equations (i.e. in *boundary integral* form). In the 1980s it became a popular tool in electromagnetic analysis.

In MoM the unknowns in the matrix equation correspond to fields (typically currents or charges) defined on surfaces rather than volumes, which leads to far fewer unknowns. Consequently, it is a very efficient method for structures with a small ratio of surface to volume. On the other hand, for problems containing large areas of material interface or complicated geometries, MoM tends to be less efficient than differential methods such as FEM.

For the deterministic analysis of periodic structures, the spectral MoM has often been used [13], [14]. In [14], a method is proposed to analyze arbitrarily shaped periodic structures composed of dielectrics and conductors which is based on the coupled volume-surface integral equation. It uses the free space periodic Green's function and solves the coupled integral equations using Rao-Wilton-Glisson (RWG) triangular elements.

The dispersion analysis of planar periodic structures by MoM is addressed in [45] and [46] for singly- and doubly-periodic structures. In [45], Bacarelli *et al.* report a novel approach which is based on a mixed-potential integral equation in a unit cell of singly periodic, microstrip structures. The integral equation is solved in the spatial domain through a triangular Delaunay mesh. In his approach, the one dimensional periodic vector and scalar Green's functions are derived in the spectral domain and an efficient sum of spectral integrals is carried out to obtain the spatial-domain quantities.

1.1.3.2 Finite difference method

FDTD is now one of the most popular computational methods in electromagnetics and over 30 commercial and university-developed FDTD based codes are available. The basic algorithm was first introduced by Yee in 1966 [18], but it was Taflove in 1980 who developed the method further and called it the "Finite-Difference Time–Domain" method. In FDTD the partial differential form of Maxwell's equations turns into a central-difference equation, applied at every node of a regular, rectangular grid. The electric and magnetic field are solved consecutively as the algorithm steps forward in time.

Being a time domain method, provided the simulation has a step size satisfying the Nyquist theorem for the highest frequency, a wide range of frequencies can be covered with a single run.

FDTD has been widely used in analyzing periodic structures [19]-[21], but only for deterministic analysis, not dispersion analysis. The periodic boundary conditions have to be imposed in the time domain. The proper way to do this is to translate the phase shift into a time shift, which can be done by dividing the length of the unit cell by the phase velocity. Then a number of time shifts are recorded at both terminal boundaries. After that, the electric and magnetic fields at the master

side update the associated fields at the slave side considering the forward time shift [22].

Despite all the merits of the FDTD method, there are some drawbacks with this method which particularly makes it less suitable for dispersion analysis of periodic structures. Stability constraints, staircase error, and the inability to consider the propagation constant as an unknown are among these drawbacks. To explain the latter more one should know that direct implementation of equation (1.5) for **E** and **H** field is technically impossible in an FDTD framework. The reason lies in the fact that such implementation results in update equations which involve unknown future values for **E** and **H**.

On the other hand the FDFD method has been applied for modal analysis of waveguide based periodic structures [47]-[49]. The problem with this method is that converting the periodic problem into a standard eigenproblem needs a mesh which is uniform in the propagation direction and also the number of meshes in this direction has to be odd [48].

1.1.3.3 Finite element method

FEM is one the most popular field analysis methods, capable of handling any kind of boundary value problem. Accuracy and ability to analyze complex three dimensional geometries are the advantages that FEM has over other numerical methods. FEM was first proposed in 1941 to solve complex elasticity and structural analysis problems in civil and aeronautical engineering, but soon found its place in many engineering fields and from 1968 was used widely in electromagnetics.

In the field of dispersion analysis of periodic microwave structures, FEM was first applied by Ferrari [23] in 1991. He proposed a FEM formulation capable of

modal analysis of a two dimensional periodic structure and generation of the corresponding dispersion curve. He validated his formulation by applying it to a ridged waveguide. Later [25]-[27], FEM formulations for periodic structures were improved but all were focused on singly periodic structures, although the geometries were three dimensional. In 1999, Mias *et al*. in [28] proposed a FEM formulation for modeling waves in doubly and triply periodic structures. They validated their formulation by applying it to 2D and 3D examples.

Despite the novelty and strength of these methods, there are many problems that cannot be solved using them. In all of them, an imaginary propagation constant is specified and the corresponding eigenvalue problem with k_0 as an unknown is solved. This *fixed-*γ approach cannot handle lossy materials. Also frequency-dependent materials and boundary conditions are very difficult to handle as their presence leads to a complicated nonlinear eigenproblem. Beyond all these difficulties, the fact of specifying a purely imaginary propagation constant and finding the corresponding frequency means that it is unable to handle the stopband of the periodic structures, where the attenuation constant is nonzero. The stopband behavior of periodic structures is important; without it there is no way of determining the degree of attenuation experienced by signals at stopband frequencies, something which is crucial, for example, in electromagnetic bandgap (EBG) power distribution networks for electronic circuits [9]. In 2007, Davanco *et al.* [30] proposed an FEM formulation to tackle this problem for 2D structures and in 2008, Tavallaee and Webb [29] introduced a formulation for 3D structures. In their fixed-k_0 approach, k_0 is specified and the problem is solved for the complex propagation constant ($\gamma = \alpha + j\beta$).

Although the approach is reliable and in theory is capable of handling any geometry and perodicity in one, two or three directions, here are two important shortcomings of the method proposed in [29]:

1) In [29] the eigenproblem is quadratic, which is more costly to solve than the more usual linear eigenproblem.

2) In [29], only dense matrix methods are used to solve the eigenproblem, making it impossible to solve realistic three-dimensional (3D) problems involving large numbers of unknowns.

The next section describes the goals of the thesis and describes how it addresses the drawbacks of the previous methods.

1.2 Research goals

The main research goal was to find a more efficient FEM to analyze dispersion in periodic structures, in both passbands and stopbands.

The first achievement was to transform the quadratic eigenvalue problem into a linear eigenproblem of the same size and then to solve the linear eigenproblem with a sparse matrix technique. In this way the complexity of the problem was reduced from $O(n^3)$ to $O(n^{1.6})$, where n is the number of unknowns, and consequently it was possible to analyze realistic 3D periodic structures for the first time.

Even with this improvement it is still time consuming to compute a dispersion curve since we have to solve a large eigenvalue problem once for each of many frequencies. In order to accelerate the overall solution a model order reduction (MOR) technique was applied to the problem. To do that, an adaptive MOR-FEM code was developed that is able to handle any kind of periodic structure in any desired frequency range.

1.3 Outline of the thesis

Chapter 2 explains the details of the approach that Tavallaee and Webb proposed in [29]. It describes the fixed-γ formulation first and then explains that this can only handle the passband of the periodic structures. The chapter continues by explaining the fixed-k_0 formulation and shows the possibility of predicting the behaviour of periodic structures both in the passband and the stopband. Chapter 2 closes by discussing the quadratic eigenvalue problem resulting from this FE formulation, the methods for solving it and their computational cost.

Chapters 3, 4 and 5 contain the three main new contributions of this thesis. These are reported in [31],[32] and [58], respectively.

Chapter 3 describes how the quadratic eigenproblem resulting from the FE formulation can be turned into a linear eigenproblem of the same size. After introducing the linear formulation the accuracy of the proposed method is verified by applying it to four different realistic structures. The chapter ends with a comparison between the computational complexities of the proposed method versus the method proposed in [29].

Chapter 4 is dedicated to a model order reduction (MOR) of the method described in chapter 3. It describes the MOR formulation and shows how the dispersion diagram over a band of frequencies can be obtained by solving the eigenproblem only for one frequency and using a Taylor series based on that expansion point. Again the accuracy of the proposed formulation is examined by analyzing different realistic examples. The computational speed-up achieved by employing the proposed method is shown as well. At the end of this chapter the limited bandwidth of MOR is discussed as a drawback of the method.

In chapter 5, a general adaptive algorithm is proposed that computes the accurate dispersion diagrams of periodic structures both in the passband and in the stopband very rapidly. The algorithm employs a smart multi-expansion point method that picks automatically the number of expansion points required to cover the desired frequency band by estimating the error caused by MOR

approximation. It also employs a tracking system for choosing the right eigenvalue for the Floquet mode under study.

The proposed algorithm is applied to five different realistic geometries and the results are validated either by comparing them to the results obtained using other techniques or comparing the results in the passband with those published in the literature. A dramatic reduction in computational is demonstrated.

Chapter 2

The finite element method for the eigen-analysis of periodic structures

The finite element method is one of the most powerful tools for the dispersion analysis of periodic structures. Although FEM has been used for this purpose for more than 20 years, it was only in 2007 that a FEM was proposed which was able to find both real and imaginary parts of the propagation constant [29] [30]. Before that, in FE formulations a purely imaginary propagation constant was specified and the corresponding frequency was sought, but in 2007, a new formulation was proposed which allows the frequency to be specified and solves an eigenvalue problem to find the complex propagation constant. In this chapter, the periodic

boundary value problem will be explained and both formulations will be discussed briefly.

2.1 Applying periodic boundary conditions to Maxwell's equations

The first step in studying the propagation of electromagnetic waves in a periodic structure is to give periodic boundary conditions for Maxwell equations and to define the boundary value problem that needs to be solved.

The phasor electric and magnetic fields, $\mathbf{E}$ and $\mathbf{H}$, are governed by the differential form of Maxwell's equations and specifically Ampere's Law

$$\nabla \times \mathbf{H} = j\omega\varepsilon\mathbf{E} \tag{2.1}$$

and Faraday's law

$$\nabla \times \mathbf{E} = -j\omega\mu\mathbf{H} \tag{2.2}$$

In the above equations, ε is the permittivity of the material and μ is the permeability. Combination of Faraday's law and Ampere's law results in a vector wave equation in either $\mathbf{E}$ or $\mathbf{H}$ that describes the propagation of the electromagnetic wave in a periodic structure. The version of the equation given in [28] is:

$$\nabla \times \frac{1}{p} \nabla \times \mathbf{F} - k_0^2 q \mathbf{F} = 0 \tag{2.3}$$

where $\omega\sqrt{\varepsilon_0 \mu_0}$ has been replaced by the free space wavenumber, k_0 . **F** on the other hand could either mean **E** or **H** depending on which field is sought. If it is **E**, then $p = \mu_r$ and $q = \varepsilon_r$ while if it is **H**, then $q = \mu_r$ and $p = \varepsilon_r$. From now on the equations will be written only for the electric field.

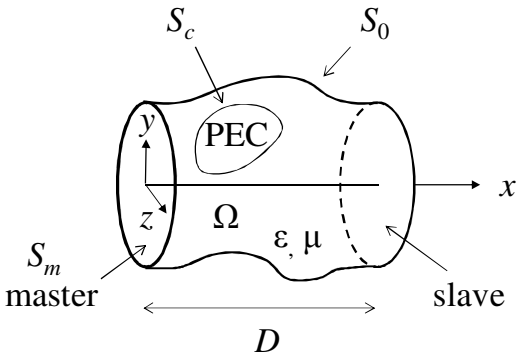

Fig. 2.1 An arbitrarily shaped unit cell of a periodic structure

Consider the structure shown in Figure 1. This structure is periodic in the *x* direction with period *D*. The geometry is totally arbitrary as long as the translation of the master surface, S_m, through distance *D* along the *x*-axis, exactly overlaps the slave surface. S_c in Fig.1 represents the surfaces which separate perfect electric conductor (PEC) from the domain, Ω. On this surface the PEC boundary condition is enforced which eliminates the unknowns on that surface ($E_t = 0$ where t denotes the tangential part). On the other hand, S_0 represents either the perfect magnetic conductor surface (PMC) or perfect electric conductor (PEC) or even another periodic constraint. In such a structure, as explained in section 1.1.1, the field **E** must satisfy the following equation:

$$\mathbf{E_t}(D, y, z) = C_x \, \mathbf{E_t}(0, y, z) \tag{2.4a}$$

where

$$C_x = e^{-\gamma D} \tag{2.4b}$$

and γ is the Floquet propagation constant. The magnetic field must satisfy a similar condition, leading to:

$$\left[\frac{1}{\mu_r}(\nabla \times \mathbf{E_t})\right]_t (x + D) = C_x \left[\frac{1}{\mu_r}(\nabla \times \mathbf{E_t})\right]_t (x) \tag{2.4c}$$

The finite element formulation of this problem aims to find the unknown $\mathbf{E}$ in the unit cell. This way, the field can be calculated all along the structure using (1.5).

2.2 FE formulation

There are two fundamental formulations of FEM, Rayleigh-Ritz and weighted residual. In this thesis the weighted residual formulation is adopted [29]. This method weights the residual of the governing differential equation and tries to

minimize the weighted residual to obtain an approximate solution for the defined domain.

The solution **F** that makes the following residual integral vanish for all weight functions **W** will also satisfy equation (2.3).

$$R = \int_{\Omega} \left(\nabla \times \mathbf{W} . \frac{1}{\mu_r} \nabla \times \mathbf{E} - k_0^2 \mathbf{W} . \varepsilon_r \mathbf{E} \right) d\Omega \tag{2.5}$$

In addition to satisfying (2.3), setting R to zero implies that the following surface integral vanishes for every weight function;

$$\oint_s \left(\mathbf{W} \times \frac{1}{\mu_r} \nabla \times \mathbf{E} \right) . \mathbf{n} ds = 0 \tag{2.6}$$

where S is the entire boundary of Ω. **E** is constrained to satisfy (2.4-a). **W** needs to be constrained as well:

$$\mathbf{W}_t(D_x, y, z) = \frac{1}{C_x} \mathbf{W}_t(0, y, z) \tag{2.8}$$

The choice $\frac{1}{C_x}$ rather than the expected C_x in this equation is necessary in order that (2-4c) follows from (2-6).

The trial function **E** and weight functions **W** have to be constrained tangentially to zero on PEC walls to satisfy boundary condition ($Et = 0\ on\ S_c$) while the PMC walls do not need any treatment as the boundary condition ($E_t = 0\ or\ (\mu_r^{-1}\nabla \times E)_t = 0\ on\ S_0$) is already satisfied in the weighted residual formulation (see (2.6)).

2.2.1 FE interpolation function

The first step in a finite element analysis is discretizing the domain into a finite number of elements of simple shape; tetrahedra are used in this thesis. This process is also called meshing. The next is selecting the interpolation functions. The interpolation functions approximate the field in each element and make sure that the solution fulfills the continuity requirements between adjacent elements. There are two types of finite element used for representing vector fields [50]: nodal elements and edge elements (sometimes called tangential vector elements). In nodal elements, the interpolation functions are associated with the nodes of the element while in edge elements they are associated with the edges and faces. Imposing continuity with nodal elements enforces continuity of both the tangential and normal parts of the vector, while imposing continuity with edge elements enforces just tangential continuity. Edge elements avoid spurious modes which usually appear when using nodal finite elements. Another advantage of edge elements is their ability to handle sudden changes in permittivity or permeability and also sharp corners of dielectric or metallic objects. For these reasons, edge elements are used in this thesis.

Consider a single tetrahedron within the mesh and call this element *e* (see Fig. 2.2).

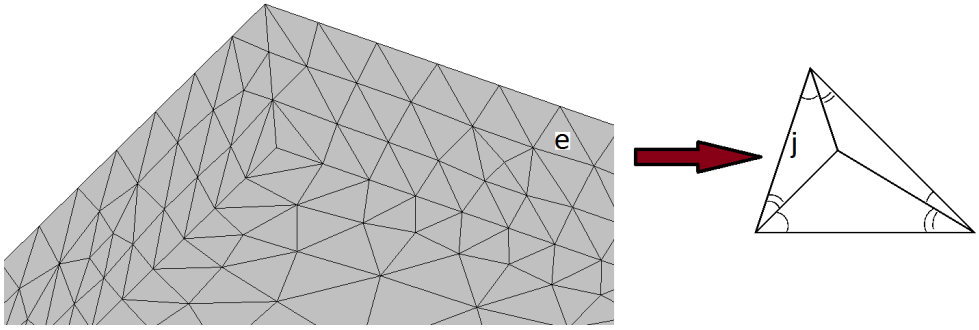

Fig. 2.2 Tetrahedral mesh and a tetrahedral element.

In this tetrahedron, we represent **E** using vector interpolation functions:

$$\mathbf{E}^{\boldsymbol{e}} = \sum_{j=1}^{l} E_j^e \mathbf{N}_\mathbf{j}^\mathbf{e} \tag{2.9}$$

In this equation, $\mathbf{N}_j^{\boldsymbol{e}}$ is a vector interpolation function and E_j^e is the scalar degree of freedom (DOF), or unknown, associated with the vector function. The interpolation functions used here are those of thehigh order, hierarchal elements described in [39]. Now if we go back to equation (2.5) where the weighted residual was introduced, we see that in order to complete the right hand side of the equation we need to have the weight functions, **W**, as well. In Galerkin's method, the weight functions are the same as the interpolation functions (also called basis functions):

$$\mathbf{W}^e = \sum_{j=1}^{l} W_j^e \mathbf{N}_j^e \tag{2.9a}$$

According to Jin [34], this choice of weight function gives the most accurate solution to the boundary value problem.

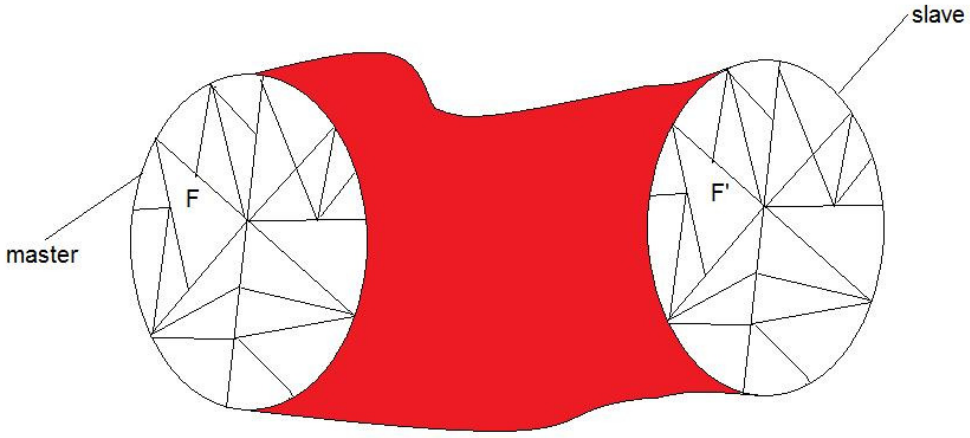

Fig. 2.3 A unit cell with an identical mesh on the master and slave surfaces.

For each $\boldsymbol{N}$ associated with unknown F on the master surface, there needs to be a matching basis function $\boldsymbol{N'}$ associated with unknown F' on the slave surface. Therefore, as seen in Fig. 2.3, it is very important to have an identical surface mesh on the master and slave boundaries. This way the unknowns associated with the slave boundary, like F', can be eliminated from the unknown list in the system of equations. Forming the system of equations will be explained in the next section.

2.2.2 Matrix assembly

So far the unit cell has been discretized into a finite number of elements and interpolation functions have been introduced to associate DOFs with the edges, faces and interior of a single element. In the next step, the DOFs in all elements are assembled into a system of equations which can be written in matrix form. This whole process is called matrix assembly.

The first matrix to be formed is the local matrix of each element. The local matrix is $l \times l$ matrix where l is the number of DOFs in one element. For example in a first order tetrahedron there are six DOFs associated with the six edges of the element. These DOFs are numbered locally from 1 to l inside each element.

Consider the part of the residual (2.5) coming from element e:

$$R^e = \int_{\Omega e} \left(\nabla \times \mathbf{W^e} . \frac{1}{\mu_r} \nabla \times \mathbf{E^e} - k_0^2 \mathbf{W^e} . \varepsilon_r \mathbf{E^e} \right) d\Omega \tag{2.10}$$

Substituting equations (2.9) and (2.9-a) in equation (2.10) and writing it in matrix form results in:

$$R^e = \{W^e\}^T ([S^e] - k_0^2 [T^e]) \{E^e\} \tag{2.11}$$

where $\{W^e\}$ and $\{E^e\}$ are $l \times 1$ column vectors containing the quantities W_j^e and E_j^e, respectively. $[S^e]$ and $[T^e]$ are $l \times l$ matrices with entries defined by :

$$S_{ij}^{e} = \frac{1}{\mu_r}\int_{\Omega^e} \nabla \times \mathbf{N_i^e}.\nabla \times \mathbf{N_j^e} d\Omega \tag{2.12}$$

$$T_{ij}^{e} = \varepsilon_r \int_{\Omega^e} \mathbf{N_i^e}.\mathbf{N_j^e}\, d\Omega \tag{2.13}$$

Since μ_r and ε_r are assumed to be uniform through the element, they have been taken outside the integral.

In addition, each DOF has a global number which determines the position of that DOF in the global FE matrix. The global FE matrix is an $n \times n$ matrix where n is the total number of DOFs in the unit cell. Of course the size of the global FE matrix is smaller than the number of elements times the number of degrees of freedom in each element, because adjacent elements share the DOFs on their common edges and faces.

The next step in the assembly process after calculating the local matrices is to sum over all elements and produce the global FE residual equation [34]:

$$R = \{W\}^T([S] - k_0^2[T])\{F\} \tag{2.14}$$

$\{F\}$ is a column vector representing all n unknowns in the unit cell and $\{W\}$ is the column vector of weights. Setting the residual to zero, we get:

$$\{W\}^T([S] - k_0^2[T])\{F\} = 0 \tag{2.15}$$

In order to impose the periodic boundary conditions (2.4a) and (2.8), the DOFs are divided into two groups: the ones lying on (i.e., controlling the tangential field on) the periodic boundaries, either on the master or slave surface, and all the rest, which will be called "interior". The DOFs are then numbered so that the interior DOFs come first, the DOFs lying on the master boundary come second and the ones lying on the slave boundary come third. The important point is that the master DOFs and the slave DOFs are numbered in exactly the same way, so that the first master DOF matches the first slave DOF, etc. The slave DOFs are now prepared to be eliminated.(In the case that doubly or triply periodic structures are being analyzed, the interior DOFs are further divided along the same lines, so that a known periodicity can be applied in, say, the y direction. For simplicity, this case will not be explicitly considered below.)

With this numbering, the slave DOFs can be eliminated from the matrix equation if we express $\{E\}$ and $\{W\}$ as follows:

$$\{E\} = [M_f]\{\hat{E}\} = \begin{bmatrix} I & 0 \\ 0 & I \\ 0 & C_x I \end{bmatrix}\{\hat{E}\}$$

$$\{W\} = [M_w]\{\widehat{W}\} = \begin{bmatrix} I & 0 \\ 0 & I \\ 0 & \frac{1}{C_x} I \end{bmatrix}\{\widehat{W}\} \tag{2.16}$$

where $\{\widehat{W}\}$ and $\{\hat{E}\}$ are reduced column vectors, containing just the interior and master DOFs. The block matrices $[M_f]$ and $[M_w]$ incorporate the periodic boundary conditions (2.4a) and (2.8), respectively.

Equation (2.15) can be rewritten as:

$$\{\widehat{W}\}^T([\hat{S}] - k_0^2[\hat{T}])\{\hat{E}\} = 0 \tag{2.17}$$

where $[\hat{S}]$ and $[\hat{T}]$ are $n \times n$ matrices given by:

$$[\hat{S}] = [M_w]^T[S][M_f] \tag{2.18}$$

$$[\hat{T}] = [M_w]^T[T][M_f] \tag{2.19}$$

and since equation (2.19) is correct for all $\{\widehat{W}\}$s, the equation to be solved is:

$$([\hat{S}] - k_0^2[\hat{T}])\{\hat{E}\} = 0 \tag{2.20}$$

The next section describes some ways of solving equation (2.20).

2.3 Solving the global system of equations

This section is dedicated to ways of solving the eigenproblem (2.20) that have been reported in the literature. The purpose of explaining these methods is to show how far the dispersion analysis of periodic structures has been addressed to date.

Equation (2.20) can represent two different eigenvalue problems. The first problem specifies the propagation constant, γ, and hence C_x, and solves for k_0^2 as the eigenvalue. This has been the traditional way to find the dispersion diagram of periodic structures.

The second eigenproblem is one that, more usefully, specifies k_0^2 and solves for C_x as the eigenvalue. This is the main contribution in [29]. The next sections explain the solution of both types of eigenproblem.

2.3.1 Solving the fixed-γ problem

Equation (2.20) can be rewritten as:

$$[\hat{S}]\{\hat{E}\} = k_0^2[\hat{T}]\{\hat{E}\} \tag{2.21}$$

This equation is a typical generalized eigenvalue problem that looks like:

$$[A]\{x\} = \lambda[B]\{x\} \tag{2.22}$$

in which A and B are $n \times n$ matrices while λ is the eigenvalue and x is the eigenvector. This kind of problem has n solutions for λ and x, i.e., in equation (2.21) we can find n eigenvalues, k_0^2, and n eigenvectors, $\{\hat{E}\}$.

The presence of multiple $k_0 s$, corresponds to the presence of multiple propagation modes in a periodic structure, i.e., for a specified propagation constant, γ, there will be n frequency points satisfying the eigenproblem.

As mentioned before, for the fixed- γ problem γ must be imaginary. The reason lies in the fact that the eigenvalue to be found in (2.21) is k_0^2, which has to be real. Choosing a purely imaginary γ, $[M_w]$ is the conjugate transpose of $[M_f]$ and the matrices [A] and [B] are hermitian, which guarantees that the eigenvalues of (2.22) are real given that [B] is a positive definite matrix. The next section explains the solution for the fixed-k_0 problem.

2.3.2 Solving the fixed-k_0 problem

In order to turn equation (2.20) into an eigenproblem with an eigenvalue that corresponds to the propagation constant, first the $[\hat{S}]$ and $[\hat{T}]$ matrices have to be expanded as follows:

$$\left[\hat{S}\right] = [M_w]^T[S]\left[M_f\right] = \begin{bmatrix} I & 0 & 0 \\ 0 & I & \frac{1}{C_x} \end{bmatrix}\begin{bmatrix} S_{11} & S_{12} & S_{13} \\ S_{21} & S_{22} & S_{23} \\ S_{31} & S_{32} & S_{33} \end{bmatrix}\begin{bmatrix} I & 0 \\ 0 & I \\ 0 & C_x \end{bmatrix}$$
$$= \begin{bmatrix} S_{11} & S_{12} + C_x S_{13} \\ S_{21} + \frac{1}{C_x} S_{31} & S_{22} + C_x S_{23} + \frac{1}{C_x} S_{32} + S_{33} \end{bmatrix} \quad (2.23)$$

$$\left[\hat{T}\right] = [M_w]^T[T]\left[M_f\right] = \begin{bmatrix} I & 0 & 0 \\ 0 & I & \frac{1}{C_x} \end{bmatrix}\begin{bmatrix} T_{11} & T_{12} & T_{13} \\ T_{21} & T_{22} & T_{23} \\ T_{31} & T_{32} & T_{33} \end{bmatrix}\begin{bmatrix} I & 0 \\ 0 & I \\ 0 & C_x \end{bmatrix}$$
$$= \begin{bmatrix} T_{11} & T_{12} + C_x T_{13} \\ T_{21} + \frac{1}{C_x} T_{31} & T_{22} + C_x T_{23} + \frac{1}{C_x} T_{32} + T_{33} \end{bmatrix} \quad (2.24)$$

[S] and [T] in (2.23) and (2.24) are in their block form. Subscripts 1, 2 and 3 represent the interior, master and slave DOFs respectively.

Group 1 includes all the unknowns of the unit cell except the ones determining the tangential electric field on the periodic boundaries. In other words this group represents the internal unknowns.

Group 2 includes the unknowns controlling the tangential electric field on the master surface.

Group 3 includes the unknowns controlling the tangential electric field on the salve surface.

One may then rewrite equation (2.20) as follows:

$$\left([M_1] + C_x[M_2] + \frac{1}{C_x}[M_3]\right)\{\hat{F}\} = (C_x[M_1] + C_x^2[M_2] + [M_3])\{\hat{F}\} = 0 \tag{2.25}$$

where

$$[M_1] = \begin{bmatrix} S_{11} - k_0^2 T_{11} & S_{12} - k_0^2 T_{12} \\ S_{21} - k_0^2 S_{21} & S_{22} + S_{33} - k_0^2 (T_{22} + S_{33}) \end{bmatrix} \tag{2.26}$$

$$[M_2] = \begin{bmatrix} 0 & S_{13} - k_0^2 T_{13} \\ 0 & S_{23} - k_0^2 T_{23} \end{bmatrix} \tag{2.27}$$

$$[M_3] = \begin{bmatrix} 0 & 0 \\ S_{31} - k_0^2 T_{31} & S_{32} - k_0^2 T_{32} \end{bmatrix} \tag{2.28}$$

The quadratic eigenvalue problem introduced in (2.25) is the main contribution of [29] which enables us to characterize the attenuation in the stopband of periodic structures, since the eigenvalue, C_x, can take complex values. The most important difficulty here is to find an efficient solution for the quadratic eigenvalue problem in (2.25). There are two main categories of quadratic eigensolvers: ones that solve the quadratic eigenvalue problem directly like the methods proposed in [36] and [37]; and ones that first convert the quadratic eigenvalue problem into a linear eigenvalue problem with matrices of double the size [35]. In [29] the second approach was chosen.

Although the second approach seems to work better for this problem, it gives a linear eigenproblem $[A]\{x\} = \lambda[B]\{x\}$ that is double-sized and has matrices [A] and [B] that are unsymmetric, complex and singular. In [29], a dense-matrix method was used to solve this problem, but this is too expensive to be able to apply to realistic three dimensional problems even for a single frequency, let alone a wide range of frequencies. As a result, only simple structures are analyzed in [29], with coarse meshes, e.g., a metal cube centered in a cubical cell.

In the following chapters it will be shown how to address this problem and an inexpensive and efficient approach to generate the dispersion diagrams for more complicated, realistic structures will be presented.

Chapter 3

Linearizing the quadratic eigenvalue problem

In the previous chapter we have seen that applying FEM to the analysis of the unit cell in a periodic structure yields a matrix equation that is linear in k_0^2 , but quadratic in γ. As explained in the previous chapters, the fixed- k_0 problem which gives the quadratic eigenproblem has significant advantages over the fixed-γ problem. However the computational cost of the fixed- k_0 approach has so far prevented the dispersion analysis of realistic 3D structures.

To address this problem, this chapter is dedicated to introducing an efficient method for solving the quadratic eigenproblem which exploits the sparsity of the FE matrices and significantly reduces the computational complexity.

3.1 The quadratic eigenvalue problem

As we saw in chapter 2, the FE formulation reported in [29] deals with the unknowns of the unit cell as three different groups: 1, 2 and 3 which represent the

interior, master and slave DOFs respectively.

This division is reflected in the global matrix, [W], in the form of 9 blocks. Each block corresponds to the interaction between two of the groups defined above.

$$[W] = \begin{bmatrix} W_{11} & W_{12} & W_{13} \\ W_{21} & W_{22} & W_{23} \\ W_{31} & W_{32} & W_{33} \end{bmatrix} \tag{3.1}$$

where $[W_{ij}] = [S_{ij}] - k_0^2[T_{ij}]$.

As discussed in the previous chapter, in order to obtain the complex propagation constant in the x-direction, the following matrix equation has to be solved, which is a quadratic eigenvalue problem (QEP) of size *n*:

$$\left([M_1] + \lambda[M_2] + \frac{1}{\lambda}[M_3]\right)\{u\} = 0 \tag{3.2}$$

where $\lambda = C_x = e^{-\gamma D}$ and

$$[M_1] = \begin{bmatrix} W_{11} & W_{12} \\ W_{21} & (W_{22} + W_{33}) \end{bmatrix} \tag{3.3}$$

$$[M_2] = \begin{bmatrix} 0 & W_{13} \\ 0 & W_{23} \end{bmatrix} \tag{3.4}$$

$$[M_3] = \begin{bmatrix} 0 & 0 \\ W_{31} & W_{32} \end{bmatrix} \tag{3.5}$$

All of these matrices are sparse.

In the next section an approach is explained which turns the quadratic eigenvalue problem into a linear eigenvalue problem of the same size where the matrices are still sparse. Moreover, unlike the alternative, double-sized linear eigenvalue problem, they are non-singular.

3.2 The linear eigenvalue problem

Consider the quadratic eigenproblem discussed in the previous section. Substituting the block form of matrices $[M_1]$, $[M_2]$ and $[M_3]$ from equation (3.3) to (3.5) into equation (3.2) gives the following:

$$\left(\lambda \begin{bmatrix} 0 & W_{13} \\ 0 & W_{23} \end{bmatrix} + \begin{bmatrix} W_{11} & W_{12} \\ W_{21} & W_{22} + W_{33} \end{bmatrix} + \frac{1}{\lambda} \begin{bmatrix} 0 & 0 \\ W_{31} & W_{32} \end{bmatrix}\right) \begin{Bmatrix} u_1 \\ u_2 \end{Bmatrix} = 0 \tag{3.6}$$

Equation (3.6) can be expanded into two equations:

$$\lambda[W_{13}]\{u_2\} + [W_{11}]\{u_1\} + [W_{12}]\{u_2\} = 0 \tag{3.7a}$$

$$\lambda[W_{23}]\{u_2\} + [W_{21}]\{u_1\} + ([W_{22}] + [W_{33}])\{u_2\} + \frac{1}{\lambda}[W_{31}]\{u_1\} + \frac{1}{\lambda}[W_{32}]\{u_2\} = 0 \quad (3.7b)$$

Multiplying equation (3.7-b) by λ it becomes:

$$\lambda^2[W_{23}]\{u_2\} + \lambda[W_{21}]\{u_1\} + \lambda([W_{22}] + [W_{33}])\{u_2\} + [W_{31}]\{u_1\} + [W_{32}\{u_2\}=0 \quad (3.8)$$

Equations (3.7-a) and (3.8) in matrix form are:

$$\left(\lambda^2\begin{bmatrix}0 & 0\\ 0 & W_{23}\end{bmatrix} + \lambda\begin{bmatrix}0 & W_{13}\\ W_{21} & W_{22}+W_{33}\end{bmatrix} + \begin{bmatrix}W_{11} & W_{12}\\ W_{31} & W_{32}\end{bmatrix}\right)\begin{Bmatrix}u_1\\ u_2\end{Bmatrix} = 0 \quad (3.9)$$

As explained in the previous section, subscripts 2 and 3 correspond to the unknowns lying on the master and slave boundaries, respectively, while subscript 1 corresponds to all the other unknowns. It is important to notice that entry *ij* of any matrix block in (3.9) is zero unless both unknowns *i* and *j* belong to the same finite element. This means that if there is a nonzero in the W_{23} block, there must be at least one finite element which contains unknowns belonging to both the master and the slave surfaces. The only way that can happen is shown in Fig. 3.1: one edge of a tetrahedron lies on one face of the cell (slave) and another edge of the same tetrahedron lies on the opposite side of the cell (master). Avoiding this case assures us that the W_{23} and W_{32} blocks are zero, which makes the coefficient of λ^2 equal to zero. One might ask how to make sure that this particular case is

avoided. The answer is that most mesh generators give an option to the user to specify the maximum length of the edges in the mesh. Simply by specifying a length smaller than the period D, this problematic case will be avoided.

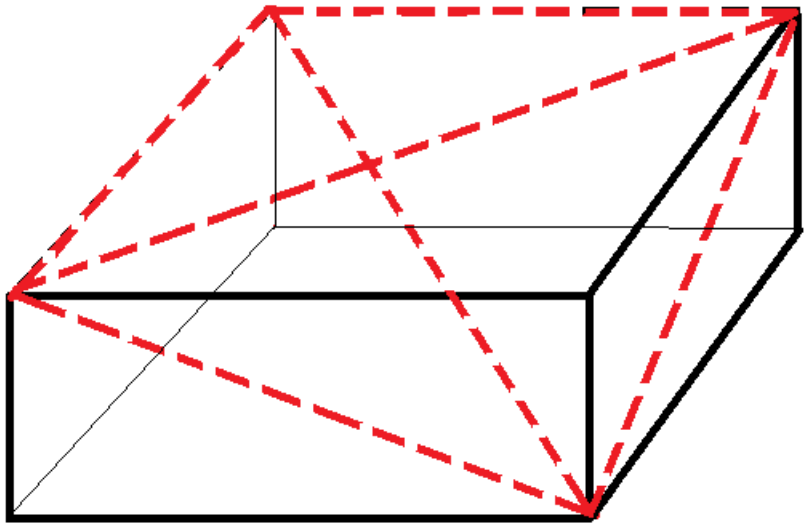

Fig. 3.1 A tetrahedron which has an edge on two opposite sides of a cube. If the cube is considered to be the unit cell in a periodic structure, this is the case that has to be avoided in order to linearize the QEP in (3.9).

Then equation (3.9) can be written as

$$\lambda \begin{bmatrix} 0 & W_{13} \\ W_{21} & W_{22}+W_{33} \end{bmatrix} + \begin{bmatrix} W_{11} & W_{12} \\ W_{31} & 0 \end{bmatrix} \begin{Bmatrix} u_1 \\ u_2 \end{Bmatrix} = 0 \qquad (3.10)$$

Equation (3.10) is a linear eigenproblem $[A]\{u\} = \lambda[B]\{u\}$ in which

$$[A] = \begin{bmatrix} W_{11} & W_{12} \\ W_{31} & 0 \end{bmatrix} \quad \text{and} \quad [B] = -\begin{bmatrix} 0 & W_{13} \\ W_{21} & W_{22} + W_{33} \end{bmatrix} \tag{3.11}$$

The important point here is that this linear eigenproblem (3.10) has the same dimension, n, as the quadratic eigenproblem (3.2). In the next section the sparse solution of this problem will be explained, leading to the calculation of dispersion curves both in the passband and the stopband.

3.3 Computing the dispersion curve

Although turning the quadratic eigenproblem into a linear generalized eigenproblem is a big step in reducing the computational cost, an efficient method for solving the linear problem can save a significant amount of additional time. A linear eigenproblem, $[A]\{u\} = \lambda[B]\{u\}$, with $n \times n$ matrices $[A]$ and $[B]$, has n eigenvalues. In the dispersion analysis of periodic structures, n eigenvalues mean n dispersion modes. Normally only one of these dispersion modes is the required one and if we can find a way to compute the associated eigenvalue directly rather than computing all n eigenvalues and then choosing the right one, we would save a huge amount of time. In fact, for efficient sparse eigensolvers the computational cost is roughly proportional to the number of eigenvalues sought.

The eigenvalue solver used in [29] is of the kind that finds all the eigenvalues at each frequency point. There are two main drawbacks with this approach:

1) the time taken to find all the eigenvalues when only one of them is needed;

and

2) the difficulty of selecting the right eigenvalue among all the eigenvalues found at each frequency, which is a manual task.

The approach proposed here to solve the eigenproblem (3.10) over a range of frequencies is to use the Arnoldi method, as implemented in MATLAB`s *eigs* function [12, 13]. Using this method, it is possible to compute only one eigenvalue at each frequency. Moreover, the *eigs* function in MATLAB has the ability to find the closest eigenvalue to a specified complex point, σ. For the first frequency point a good guess is given for the propagation constant of the desired mode and σ is set to the C_x value corresponding to that. The σ at subsequent frequency points is set to be the eigenvalue of the previous frequency point. Choosing a small frequency step makes it very likely that the eigenvalue does not change much from one point to the next and so this technique will successfully track the desired mode. The challenge is to find the right value of σ for the first frequency.

In order to address this challenge, the initial σ is calculated by solving the fixed γ problem (2.21) for the lowest few modes and selecting the desired mode. The fixed γ problem is solved for an arbitrary γ in the passband (e.g., $j\frac{\pi}{2}$) and the associated frequency is found. Depending on the location of that frequency point, the frequency sweep is made toward the right or toward the left, or both, until the required range is covered. In this way, we can have the dispersion diagram automatically for any range of frequencies.

The Arnoldi method solves the following linear matrix equation at each iteration:

$$([A] - \sigma[B])\{u\} = [B]\{v\} \tag{3.12}$$

The equation is solved for $\{u\}$, while the vector $\{v\}$ is known. Equation (3.12) can be either solved directly using MATLAB's "\" operator, which employs a sparse direct method, or iteratively using the different Krylov methods available in

MATLAB. Using the direct solver was less expensive for the test cases reported in this thesis.

3.4 Results

This section shows the capability of the new method. A comparison in CPU time is made between the new method and the method reported in [29]. The comparison is only made for three simple structures as this is all that is possible using the method in [29], but afterwards the dispersion curves of three other, more realistic, periodic structures are presented.

3.4.1 Computational complexity comparison

As mentioned in chapter 2, the largest problem analyzed with the method of [29] was a cubic unit cell containing a centrally-placed metallic cube. In this section, the computational times of the solution of the quadratic eigenproblem (3.2) using the MATLAB function *polyeig* is compared with the computational time of the new method.

Fig. 3.2 shows the dramatic reduction in computation time using the new method. This figure gives the CPU time for the analysis of three structures described in [29]. These are, respectively, singly periodic, doubly periodic and triply periodic, and all are analyzed in 3D with tetrahedral finite elements, all first order. The matrix dimension, n, for these structures is 345, 900 and 2960, respectively. The triply periodic problem is the metallic cube problem. The length of the unit cell in this problem is 10 mm while the length of the centered metallic cube is 1 mm. The timings for this and subsequent figures are for finding one point of the dispersion curve. The computer is a P8700 Dual Core processor

running at 2.53 GHz.

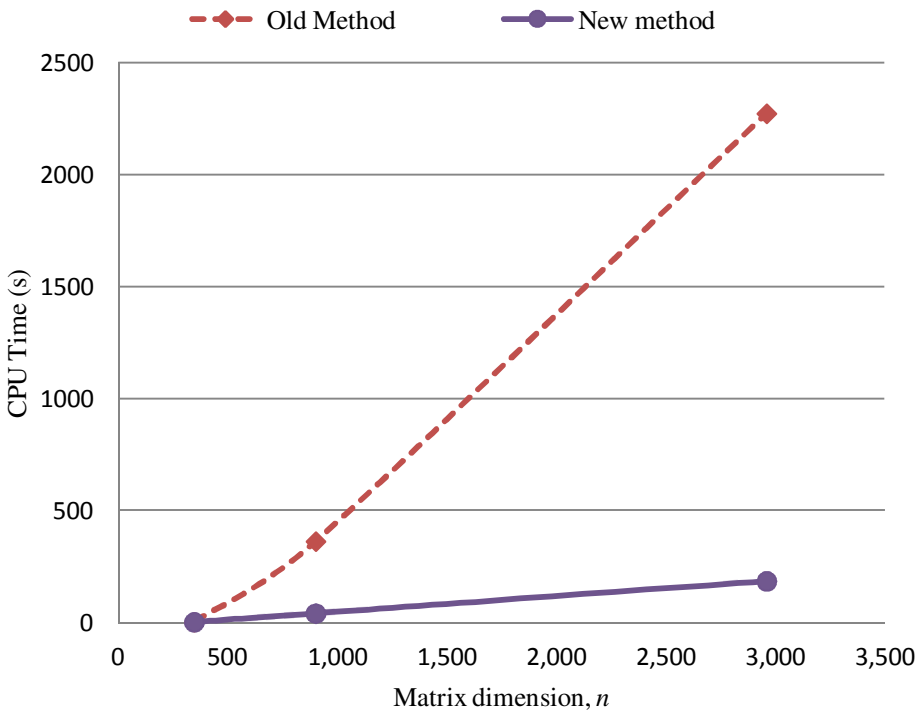

Fig. 3.2 Comparison of the CPU times of the new method and the old method [29].

Fig. 3.3 shows the variation of the CPU time versus n, for problems obtained by refining the mesh for the metallic cube problem (Fig. 5 of [29]). The problem is analyzed with finite elements at first, second and third orders. Linear regression gives the slopes of the three lines in Fig. 2 as 1.31, 1.45 and 1.54, respectively, indicating a growth of CPU time with n that is slower than $n^{1.6}$.

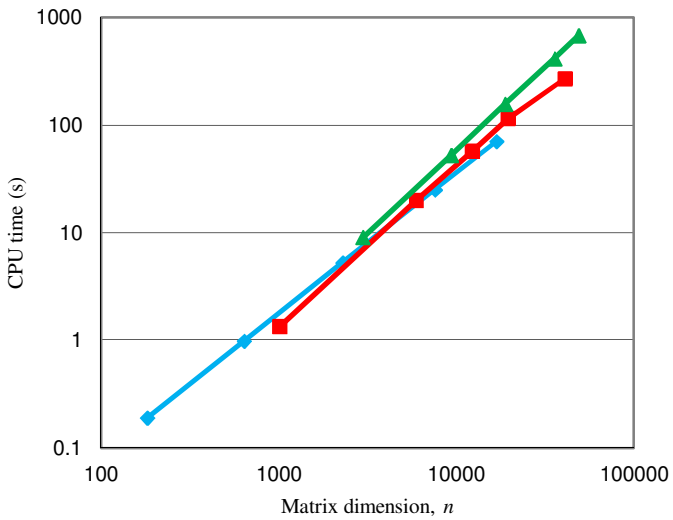

Fig. 3.3 The variation of CPU time of the metallic cube problem for first, second and third order elements. The blue diamonds, red squares and green triangles correspond to element orders one, two and three, respectively.

Fig. 3.4 shows the dispersion diagrams for the metallic cube problem, both for the phase and attenuation constants (β and α, the imaginary and real parts of γ, respectively). The results obtained using the new method agree closely with the results in [29], showing that the efficiency of the new method does not come at the cost of any loss of accuracy.

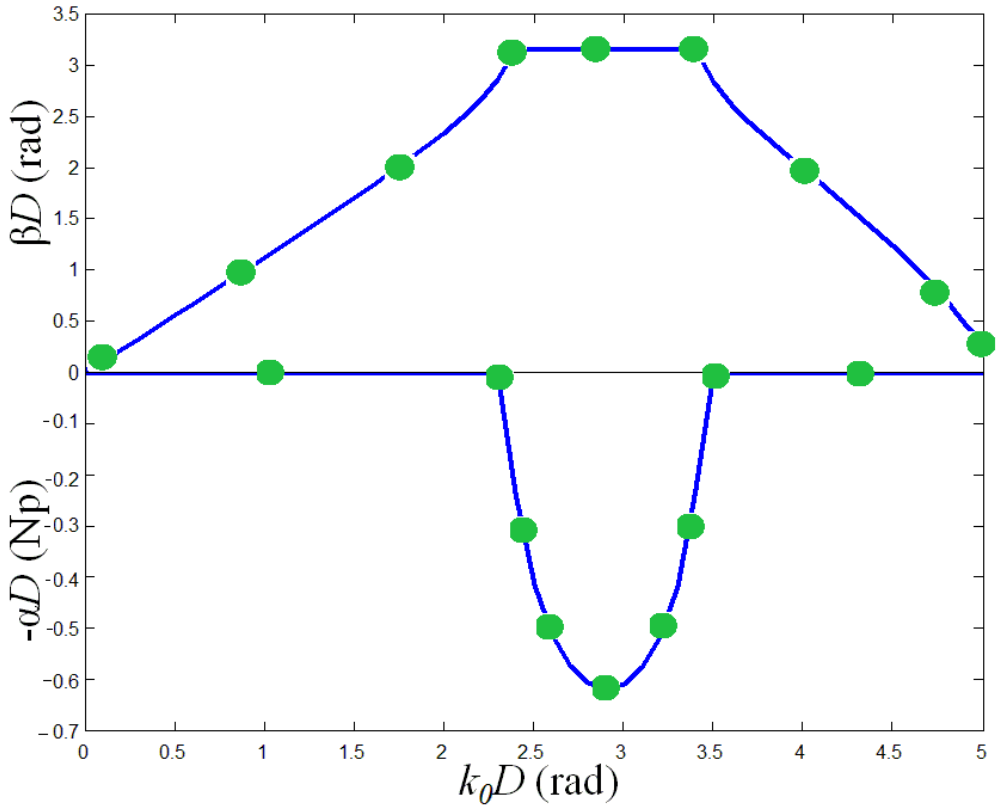

Fig. 3.4 Complex propagation constant of the metallic cube problem. The lines correspond to the new method while the circles correspond to the results reported in [29]. For this problem the step size for k_0D is 0.1. There are 1,925 elements of order 3. The matrix size, n, is 35,500.

3.4.2 Results for the dispersion analysis of other structures

The most important benefit of the new method is that it gives us the ability to compute the dispersion curve for realistic structures, which was impossible using the previous method. In this section, three realistic periodic structures are analyzed using the new method and the results are validated by comparing the phase constant in the passband of the structures with results from the published literature. Attenuation constants are also presented, even though no comparison with previously published results is possible.

3.4.2.1 Mushroom structure

Fig. 3.5 shows a widely-used periodic structure called a mushroom structure [9].

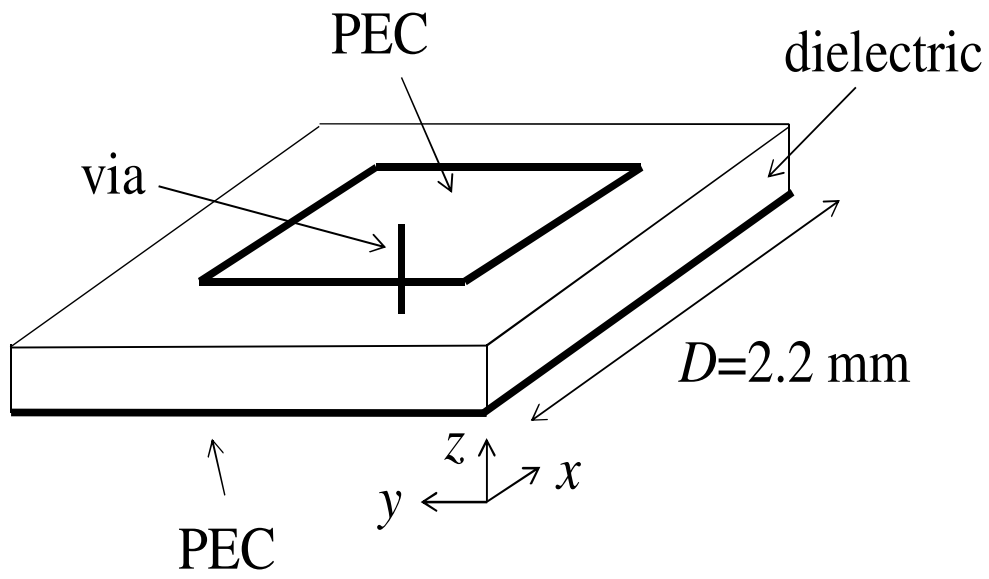

Fig. 3.5 Unit cell of the mushroom structure. The unit cell is a square in the xy plane. The side of the metallic square patch is 2mm.

The main application of this is in power distribution networks (PDN) where they are used as ground planes [9]. As can be seen in Fig. 3.5, the mushroom structure is formed of a square, metallic surface printed on a dielectric substrate and connected to a metal plane with a narrow metallic via. The metal is modeled as perfect electric conductor (PEC). The structure is three dimensional and doubly periodic, in the x and y directions. Fig. 3.6 shows the side view of the structure.

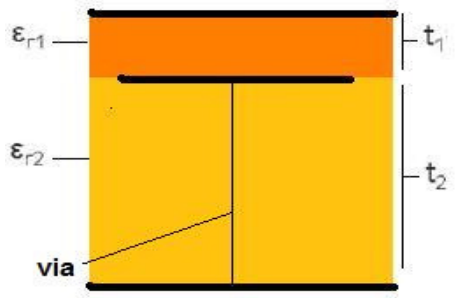

Fig. 3.6 The side view of the mushroom structure. The black lines indicate PEC. In this figure: ε_{r1} = 30, ε_{r2}= 2.33, t_1 = 0.016 mm, t_2 = 0.1 mm, via diameter = 0.125 mm.

Fig. 3.7 shows the dispersion curves of the mushroom structure both in the passband and the stopband.

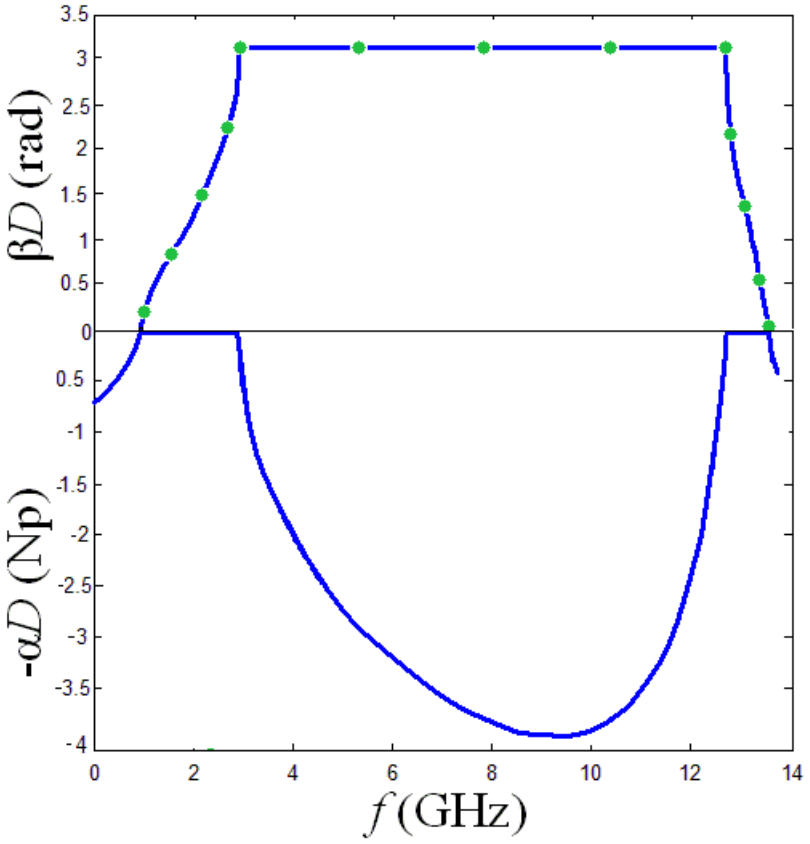

Fig. 3.7 Complex propagation constant of the mushroom structure (Figs. 3.5 and 3.6). The lines correspond to the new method while the circles correspond to the results reported in [9]. The frequency step size is 0.1 rad/m and the elements are third order. The number of elements used is 2,047 and the matrix size is 32,232.

The propagation constant shown in Fig. 3.7 is actually the propagation constant in the x direction when it is set to zero in the y direction. The results in the passband are compared with the results reported in [9] which are obtained using commercial FEM software, HFSS from Ansys [51].

To check the computational complexity of the method, the increase in CPU time as the matrix size grows is plotted in Fig. 3.8. The growth in matrix size is obtained by refining the mesh. Linear regression gives the slopes of the three lines as 1.53, 1.57 and 1.55 for the first, second and third orders, respectively.

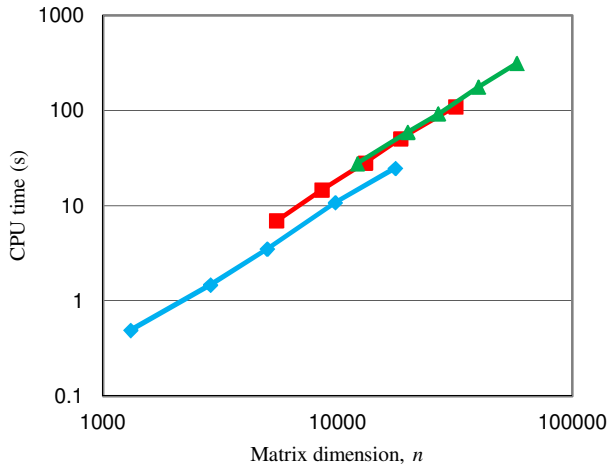

Fig. 3.8 The variation of CPU time of the mushroom problem for first, second and third order elements. The blue diamonds, red squares and green triangles correspond to element orders one, two and three, respectively.

3.4.2.2 LPC-EBG structure

The long period coplanar electromagnetic band gap (LPC-EBG) structure is another popular periodic structure which is used to isolate the power noise in PDNs [40]. Like the mushroom, the unit cell of an LPC-EBG structure is formed of a metallic pattern printed on a dielectric substrate. Fig. 3.9 shows an LPC-EBG structure.

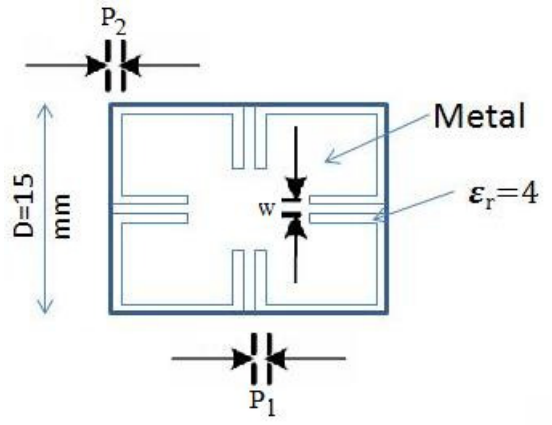

Fig. 3.9 The top view of the square unit cell of LPC-EBG structure. The metallic patch is printed on a FR4 substrate with relative permittivity of 4 and thickness 1.6 mm [40]. $P_1 = P_2 = w = 0.5mm$.

This structure is analyzed using the new method. The dispersion diagram is depicted in Fig. 3.10. The propagation constant shown in Fig. 3.10 is for the x direction; the propagation constant in the y direction is set to $j\pi$. Like the mushroom structure, only the results in the passband are validated, by comparing with the results obtained by commercial FEM software. The results in the stopband are generated for the first time.

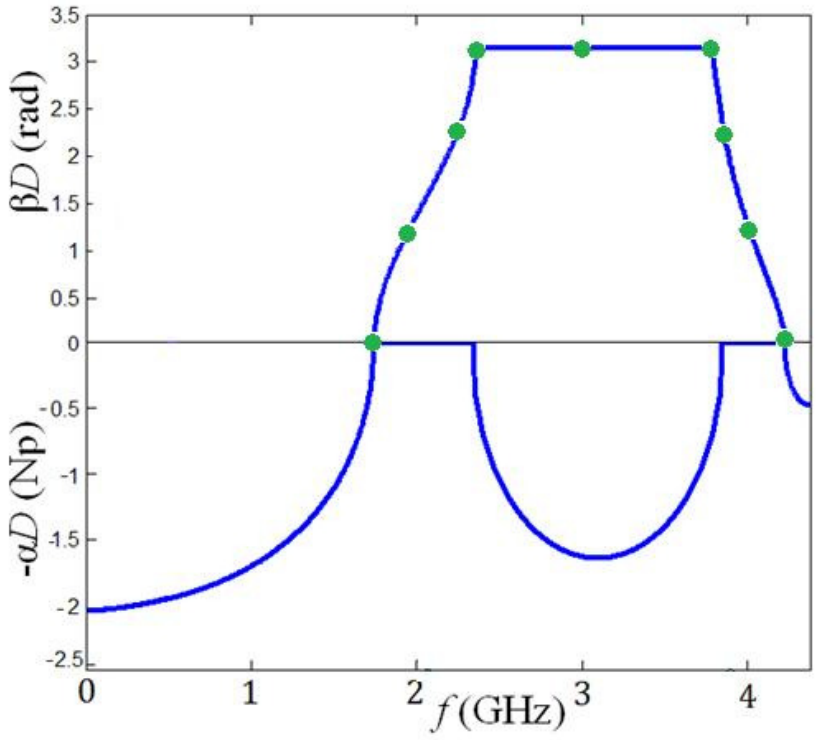

Fig. 3.10 Complex propagation constant of the LPC-EBG structure. The lines correspond to the new method while the circles correspond to the results reported in [40]. The frequency step size is 0.1 rad/m and the elements are third order. The number of elements used is 1,032 and the matrix size is 19,968.

3.4.2.3 AS-EBG structure

The artificial substrate EBG (AS-EBG) structure is another structure designed to suppress the switching noise on PDNs [40]. It is designed by periodically embedding high and low dielectric constant rods in the LPC-EBG structure (Fig. 3.9), through the full height of the dielectric substrate. The geometry of the AS-EBG structure is depicted in Fig. 3.11.

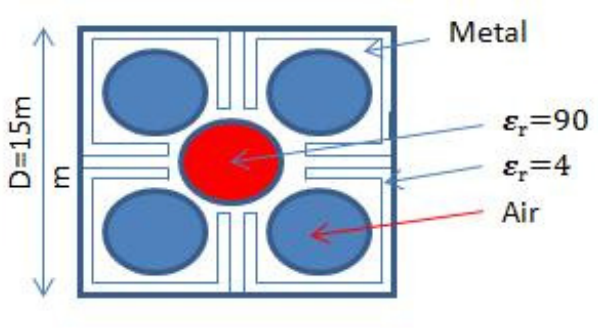

Fig. 3.11 The top view of the unit cell of the AS-EBG structure. The metallic patch has the same dimensions as the LPC-EBG structure and the substrate is the same as well (t=1.6mm, ε_r=4).

The AS-EBG structure is analyzed by the new method and the phase constant and the attenuation constant is computed for a frequency band between 0 and 5.5 GHz. The dispersion diagram of the AS-EBG structure is shown in Fig. 3.12. The propagation constant in Fig. 3.12 is for the x direction; the propagation constant in the y direction is set to $j\pi$. Like the other two structures in this section, the passband results are validated against HFSS results. The stopband results are generated for the first time.

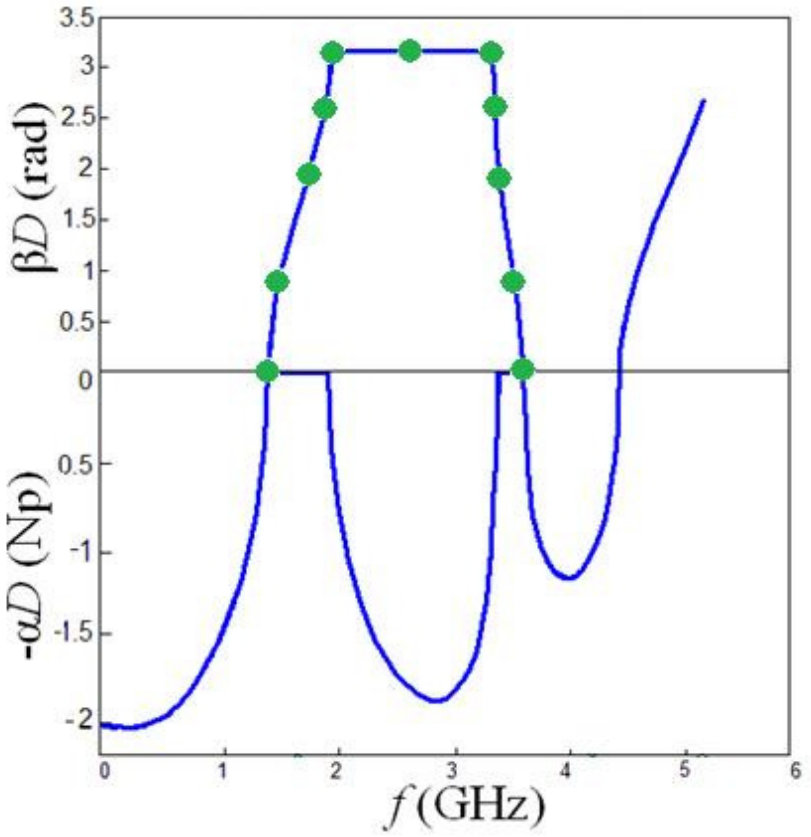

Fig. 3.12 Complex propagation constant of the AS-EBG structure. The blue line corresponds to the proposed method in this chapter while the green circles correspond to the results reported in [40]. The frequency step size is 0.1 rad/m and the elements are third order. The number of elements used is 2,247 and the matrix size is 46,530.

Chapter 4

A Model-Order Reduction Method for the Passband and Stopband

As discussed in the previous chapters, the finite element method (FEM) has been applied very successfully to the analysis of the unit cell of periodic structures. The original FEM specifies a purely imaginary γ and finds the corresponding frequency, which gives the passband behavior, but not the stopband [28] [38]. The FE formulation introduced in [29] allows the frequency to be specified and the resulting complex γ to be computed, though the method is not really practical because it involves a quadratic eigenproblem. This problem was solved with the

linearization technique described in chapter 3. With this technique, both the passband and the stopband of periodic structures can be explored.

Getting the curves of γ versus frequency requires stepping through the frequency band in small increments. Since an eigenvalue problem must be solved at each frequency, the overall computational cost is still very high for realistic three dimensional geometries. This chapter is dedicated to introducing a model-order reduction (MOR) technique to reduce considerably the cost of the frequency sweep.

MOR is an established concept in science and engineering. Often, simulating realistic systems results in high-dimensional mathematical models. Therefore engineers and scientist always look for the simplest mathematical model that is still capable of providing the required data. One solution is MOR, which is the systematic way of reducing the dimensionality. Dealing with lower dimensional models simplifies the analysis and simulation. MOR has been successfully employed to solve large-scale problems in control engineering [53], signal processing [54], circuit simulation [55] and many other areas of engineering.

In the field of electromagnetics, MOR has been applied to the 2-D waveguide mode problem [41][42], making use of a Taylor series expansion at one frequency point. It was also applied to the analysis of periodic structures in [43], but only for the fixed-γ problem.

In this chapter MOR is applied to the fixed-k_0 problem. It is a single point technique, similar to what has been used for the 2-D waveguide mode problem [41][42]. The first section of this chapter reviews briefly the FE analysis of periodic structures while the second section explains in detail the procedure for obtaining the reduced order model. The results of applying MOR to the FE analysis of some periodic structure are shown and discussed in the last section.

4.1 Review of FE analysis of periodic structures

In the previous chapter it was seen that once the FE global matrix is obtained, it is partitioned as follows:

$$[W] = \begin{bmatrix} W_{11} & W_{12} & W_{13} \\ W_{21} & W_{22} & W_{23} \\ W_{31} & W_{32} & W_{33} \end{bmatrix} \tag{4.1}$$

To conduct a fixed-k_0 analysis, the following eigenproblem needs to be solved:

$$[A]\{x\} = \lambda[B]\{x\} \tag{4.2}$$

where

$$\lambda = e^{\gamma_D} \tag{4.3}$$

and $[A]$ and $[B]$ are these complex, asymmetric and sparse $n \times n$ matrices:

$$[A] = \begin{bmatrix} W_{11} & W_{12} \\ W_{31} & 0 \end{bmatrix} \tag{4.4}$$

$$[B] = -\begin{bmatrix} 0 & W_{13} \\ W_{21} & W_{22} + W_{33} \end{bmatrix} \tag{4.5}$$

As explained in chapter 3, the matrix [W] is frequency dependent. Each block takes the form:

$$[W_{ij}] = [S_{ij}] - k_0^2[T_{ij}] \tag{4.6}$$

$[S_{ij}]$ and $[T_{ij}]$ are k_0-independent matrices. Consequently, $[A]$ and $[B]$ can be written as

$$[A] = [A_S] - k_0^2[A_T] \tag{4.7}$$

$$[B] = [B_S] - k_0^2[B_T] \tag{4.8}$$

where $[A_S]$, $[A_T]$, $[B_S]$ and $[B_T]$ are k_0-independent matrices. The following section describes the details of applying MOR to the eigenvalue problem (4.2) using the expansion of these matrices around a specified wavenumber.

4.2 Applying MOR

This section describes the application of MOR to the FE analysis of periodic structures. The method is similar to that proposed for the 2D FE analysis of waveguide modes [41].

In equations (4.7) and (4.8), the frequency dependence of the matrices [A] and [B] is shown. Using equation (4.7), matrix [A] can be expanded about a chosen wavenumber, k_e:

$$[A] = \sum_{i=0}^{2} [A_i](\Delta k_0)^i \tag{4.9}$$

where

$$\begin{aligned} \Delta k_0 &= k_0 - k_e \\ [A_0] &= [A_S] - k_e^2[A_T] \\ [A_1] &= -2k_e[A_T] \\ [A_2] &= -[A_T] \end{aligned} \tag{4.10}$$

The matrix $[B]$ can be expanded the same way.

The next step is to expand the unknowns $\{x\}$ and λ as Taylor series in Δk_0. The unknowns can be written as:

$$x = \sum_{i=0}^{\infty} x_i (\Delta k_0)^i \tag{4.11}$$

$$\lambda = \sum_{i=0}^{\infty} \lambda_i (\Delta k_0)^i \tag{4.12}$$

Now that the all parameters and matrices are expanded, they can be substituted into equation (4.2). Equation (4.2) can be rewritten as:

$$\begin{aligned} &\left(\sum_{i=0}^{2} [A_i](\Delta k_0)^i]\right)\left(\sum_{i=0}^{\infty} x_i (\Delta k_0)^i\right) \\ &= \left(\sum_{i=0}^{\infty} \lambda_i (\Delta k_0)^i\right)\left(\sum_{i=0}^{2} [B_i](\Delta k_0)^i]\right)\left(\sum_{i=0}^{\infty} x_i (\Delta k_0)^i\right) \end{aligned} \tag{4.13}$$

Equation (4.13) is a polynomial in Δk_0. To solve the equation approximately we can equate the term in the p^{th} power of Δk_0 on both sides. This yields:

$$[A_0]\{x_0\} = \lambda_0 [B_0]\{x_0\}$$

$$\& \tag{4.14}$$

$$[M]\{x_p\} = \lambda_p\{w\} + \{v\} \qquad p=1,2,\ldots$$

where

$$[M] = [A_0] - \lambda_0[B_0] \tag{4.15}$$

and $\{w\}$ and $\{v\}$ are n-vectors which can be calculated from $\{x_i\}$ and λ_i for $i = 1, \ldots, p-1$:

$$\{w\} = [B_0]\{x_0\} \tag{4.16}$$

$$\{v\} = -\sum_{i=1}^{\min(2,p)} ([A_i] - \lambda_0[B_i])\{x_{p-i}\} + \sum_{i=1}^{p-1} \lambda_i \cdot \sum_{j=0}^{\min(2,p-i)} [B_j]\{x_{p-i-j}\} \tag{4.17}$$

To find the starting values x_0 and λ_0 the eigenproblem (4.2) has to be solved at $k_0 = k_e$. Then x_p and λ_p can be found from (4.14), in the following way. $[M]$ in (4.14) is singular, having one right null-vector $\{x_0\}$, corresponding to the solution at $k_0 = k_e$. Therefore (4.14) is only soluble if the right-hand side lies in the column space of $[M]$. This can be guaranteed by choosing λ_p to satisfy the following equation:

$$\{u_0^H\}\left(\lambda_p\{w\} + \{v\}\right) = 0 \tag{4.18}$$

where H stands for hermitian (i.e., conjugate transpose). In this equation, $\{u_0\}$ is the left null-vector of $[M]$ and is obtained by solving a second eigenproblem, with a known eigenvalue:

$$[A_0]^H\{u_0\} = \lambda_0^H\,[B_0]^H\{u_0\} \tag{4.19}$$

Once $\{u_0\}$ is found, (4.18) can be solved for λ_p, and then equation (4.14) can be solved for $\{x_p\}$.

However, since [M] is a singular matrix, equation (4.14) cannot be solved directly. In order to tackle this problem, in [41] the row and column corresponding to the largest entry of $\{x_0\}$ is eliminated to make the matrix non-singular. However that method was not found to work well in the present case. Instead, equation (4.14) is solved iteratively using the bi-conjugate gradient method with LU preconditioning employing threshold partial pivoting [52]. The LU preconditioning is based not on $[M]$, but on the non-singular matrix $[M] - \theta\lambda_0[B_0]$, where $\theta \ll 1$. The value $\theta = 0.01$ was used for the results in this thesis.

Once vectors $\{x_p\}$ for $p = 0, \dots, P$ have been computed, an orthonormal set of $L \leq P + 1$ vectors is found that spans the same space as the $\{x_p\}$. The orthonormality is achieved using QR decomposition. The L vectors are placed in the columns of an $n \times L$ matrix $[E]$. $[E]$ is the matrix that achieves the ultimate dimension reduction. $[E]^H$ and $[E]$ are multiplied by both $[A]$ and $[B]$ from the left and right side. This way the size of the eigenproblem is reduced from n to L:

$$([E]^H[A][E])\{y\} = \lambda([E]^H[B][E])\{y\} \tag{4.20}$$

where $\{y\}$ is an L-vector. Since L is typically in the range 5 to 20, the eigenproblem (4.20) can be solved very quickly at each frequency over the range of interest. Solving equation (4.20), gives all L eigenvalues. To track the dispersion curve, the closest eigenvalue to the one found for the previous frequency point is selected.

4.3 Results

The method described in chapter 2 was only able to analyze very simple structures like the metallic cube, while the method introduced in chapter 3 enabled us to analyze more complicated 3-D structures. In this chapter, the four periodic structures analyzed in chapter 3 (the metallic cube, the mushroom, the LPC-EBG and the AS-EBG) are analyzed again using MOR. The results obtained are compared with those obtained in chapter 3. Also, the computational cost (CPU time) of the MOR analysis is compared with the cost of solving without MOR. The dispersion curves presented is this section are computed using a similar eigenvalue tracking technique to the one used in chapter 3 with this difference: in chapter 3, the *eigs* function found the closest eigenvalue to the eigenvalue of the previous frequency point, while here all the eigenvalues of the reduced matrix are found and the code selects the one that is closest to the eigenvalue of the previous frequency point.

4.3.1 The metallic cube

Fig. 4.1 shows the dispersion curve of the cube structure when the expansion point $k_e D = 2$ rad is in the passband of the periodic structure. The MOR results are obtained by solving the FE model at the expansion point and obtaining $\{x_p\}$ vectors up to P=20. Orthogonalizing the vectors gives 20 linearly independent vectors out of 21 $\{x_p\}$ vectors, i.e., for this problem L=20. Then the reduced order model (the 20×20 eigenproblem) is solved.

As can be seen, the MOR results closely match the ones obtained in chapter 3. The maximum difference in γD between the two sets of results shown in the figure is 10^{-3}.

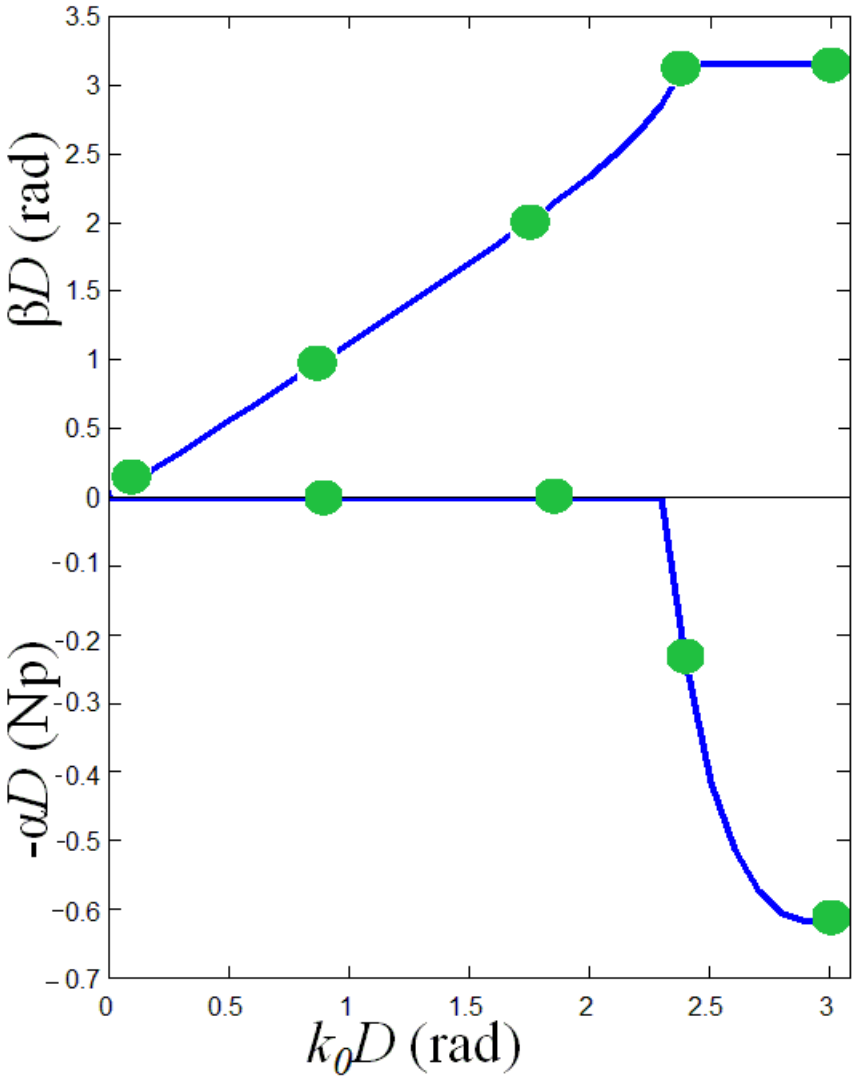

Fig. 4.1 The dispersion curve of the metallic cube problem. The straight line corresponds to the MOR results while the circles correspond to the results obtained in chapter 3. The step size for the MOR results, for $k_0 D$, is 0.01. There are 1,925 elements of order 3. The matrix size, n, is 35,500.

Fig. 4.2 gives results for the same structure with this difference, that the expansion point is now $k_e D = 2.5$ rad, which is in the stopband. As can be seen here as well, the results match the ones obtained in chapter 3; the maximum difference in γD is again 10^{-3}. The reason for including this figure is to show that MOR works equally well whether the expansion point is in the passband ($k_e D$ =2 rad) or in the stopband ($k_e D$ =2.5 rad).

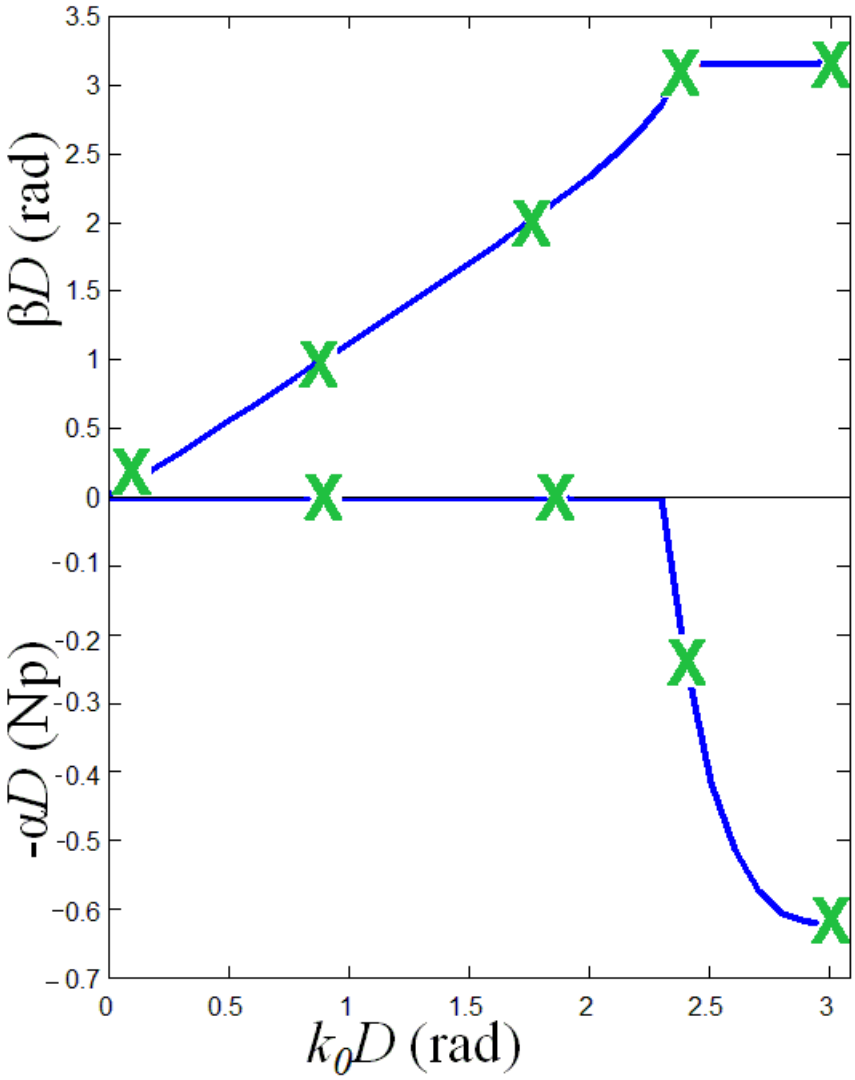

Fig. 4.2 The dispersion curve of the metallic cube problem. The straight line corresponds to the MOR results while the crosses correspond to the results obtained in chapter 3. The step size for the MOR results, for $k_0 D$, is 0.01. There are 1,925 elements of order 3. The matrix size, n, is 35,500.

4.3.2 The mushroom structure

As in the previous case, the MOR is tried once with the expansion point in the passband and once with the expansion point in the stopband. Fig. 4.3 shows the dispersion diagram of the mushroom structure when the expansion point is in the passband, at $f = 2.38$ GHz. As can be seen, the results match the ones obtained in chapter 3; the maximum difference is 10^{-4}.

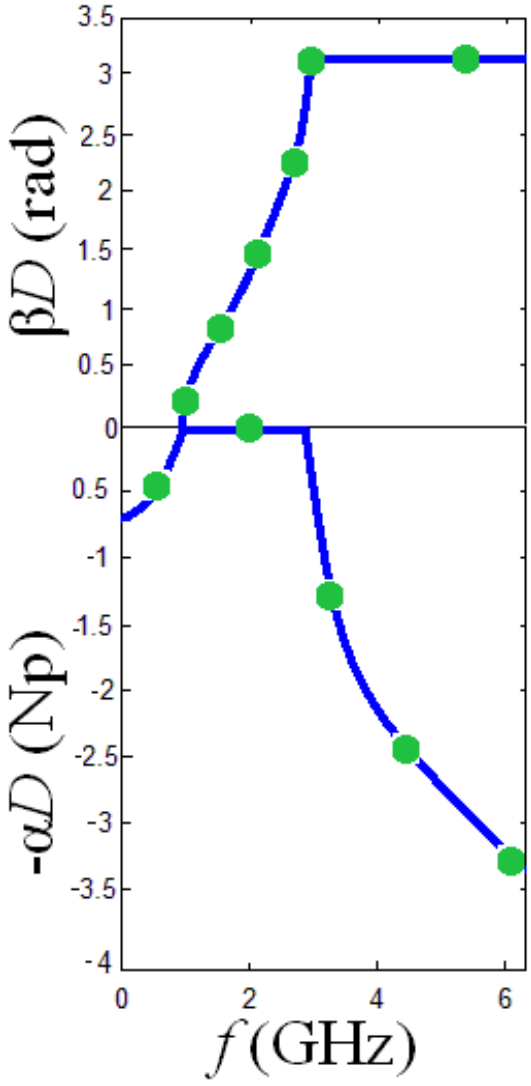

Fig. 4.3 The dispersion curve of the mushroom structure with the expansion point in the passband. The straight line corresponds to the MOR results while the circles correspond to the results obtained in chapter 3. The frequency step size for the MOR results is 0.01 rad/m and the elements are third order. The number of elements used is 2,047 and the matrix size is 32,232.

The MOR results are obtained by solving the FE model at the expansion point and obtaining $\{x_p\}$ vectors up to P=15. Orthogonalizing the vectors gives 14 linearly independent vectors out of 16.

Fig. 4.4 shows the dispersion diagram of the same structure with the expansion point located in the stopband at $f = 3.1$ GHz.

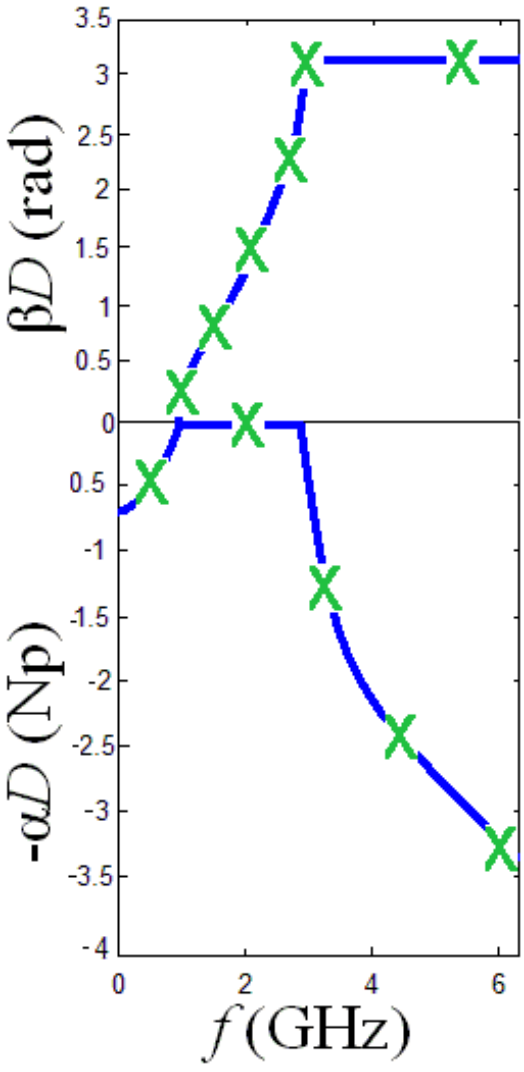

Fig. 4.4 The dispersion curve of the mushroom structure with the expansion point in the stopband. The straight line belongs to the MOR results while the crosses belong to the results obtained in chapter 3. The

frequency step size for the MOR results is 0.01 rad/m and the elements are third order. The number of elements used is 2,047 and the matrix size is 32,232.

4.3.3 The LPC-EBG structure

Fig. 4.5 shows the dispersion curve of the LPC-EBG structure when the expansion point is inside the passband, at $f = 2$ GHz. The MOR results are obtained by solving the FE model at the expansion point and obtaining $\{x_p\}$ vectors up to P=15. Orthogonalizing the vectors gives 12 linearly independent vectors out of 16.

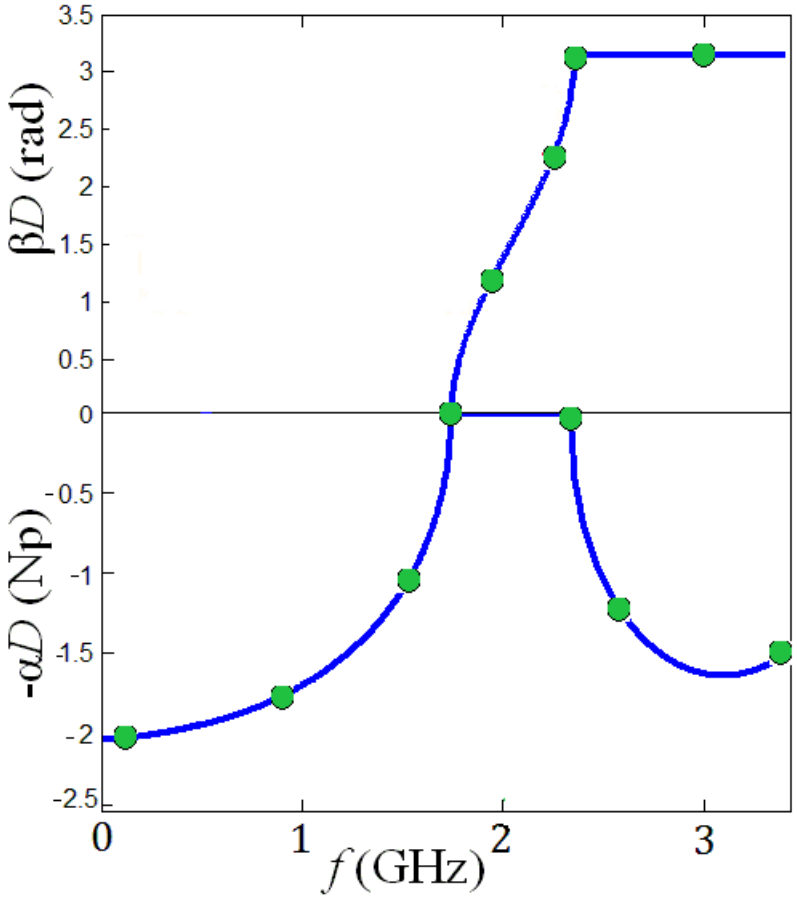

Fig. 4.5 The dispersion curve of the LPC-EBG structure with the expansion point in the passband. The straight line belongs to the MOR results while the circles belong to the results obtained in chapter 3. The

frequency step size for the MOR results is 0.01 rad/m and the elements are third order. The number of elements used is 1,032 and the matrix size is 19,968.

Fig. 4.6 shows the dispersion curves of the same structure when the MOR expansion point is located in the stopband, at $f = 1.5$ GHz. As can be seen, the results match the ones obtained in chapter 3; the maximum difference is 10^{-3}.

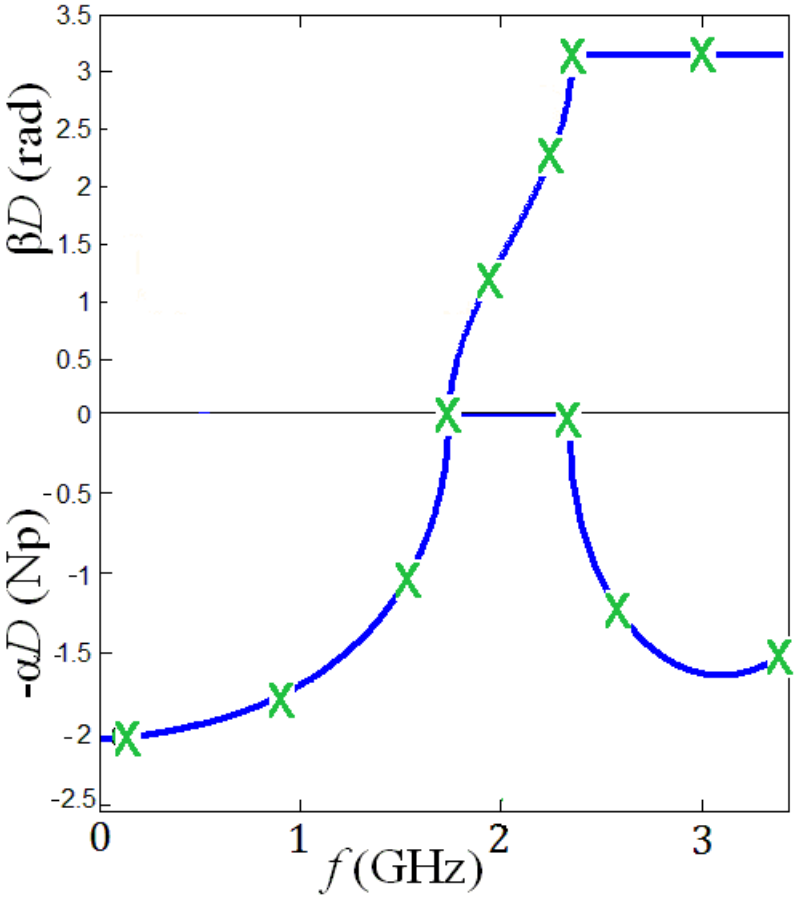

Fig. 4.6 The dispersion curve of the LPC-EBG structure with the expansion point in the stopband. The straight line belongs to the MOR results while the crosses belong to the results obtained in chapter 3. The frequency step size for the MOR results is 0.01 rad/m and the elements are third order. The number of elements used is 1,032 and the matrix size is 19,968.

4.3.4 AS-EBG structure

Fig. 4.7 shows the dispersion curve of the AS-EBG structure with the expansion point in the passband, at $f = 1.8$ GHz.

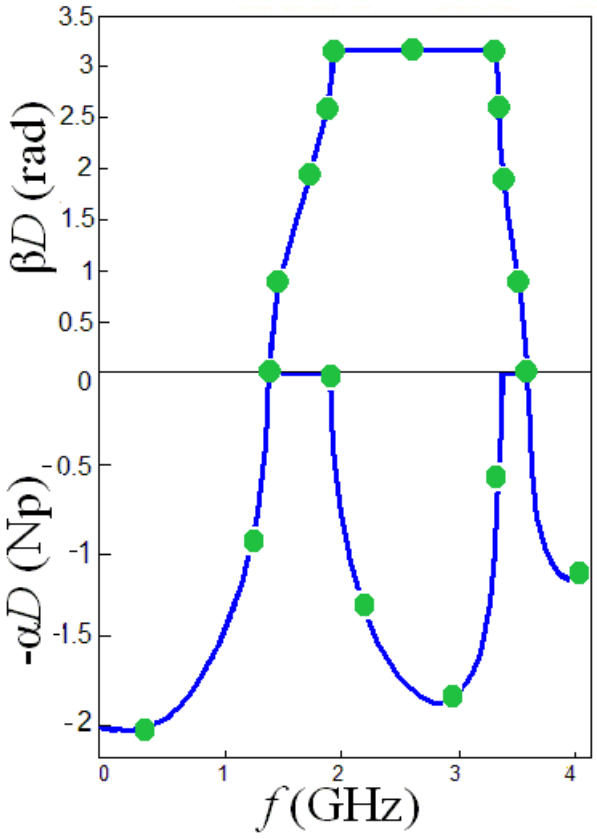

Fig. 4.7 Dispersion curve of the AS-EBG structure with the expansion point in the passband. The straight line belongs to the MOR results while the circles belong to the results obtained in chapter 3. The frequency step size for the MOR results is 0.01 rad/m and the elements are third order. The number of elements used is 2,247 and the matrix size is 46,530.

The MOR results are obtained by solving the FE model at the expansion point and obtaining $\{x_p\}$ vectors up to P=15. Orthogonalizing the vectors gives 11 linearly independent vectors out of 16 .

Fig. 4.8 shows the dispersion curve of the structure when the expansion point is inside the stopband, at $f = 2.2$ GHz.

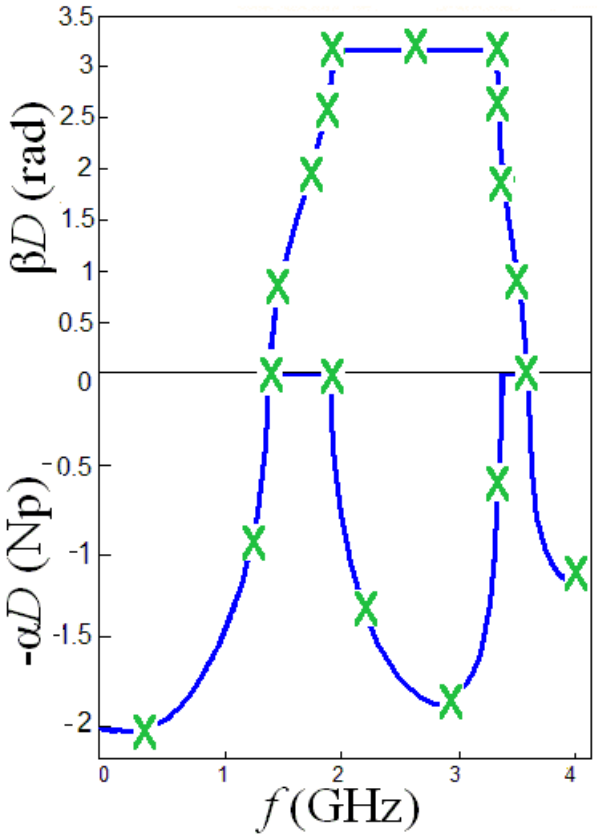

Fig. 4.8 The dispersion curve of the AS-EBG structure with the expansion point in the stopband. The straight line belongs to the MOR results while the crosses belong to the results obtained in chapter 3. The frequency step size for the MOR results is 0.01 rad/m and the elements are third order. The number of elements used is 2,247 and the matrix size is 46,530.

The results match the ones obtained in chapter 3 with a maximum difference of 10^{-3}.

4.3.5 Computation Time

The main purpose of MOR is to reduce the computational cost. Table 1 shows the computational costs of analyzing the four structures. The table compares the cost of solving the eigenproblem using the method introduced in chapter 3 (the "direct" method) with the cost of solving the same problem using the MOR method explained in this chapter. As seen in the table, the cost is greatly reduced by using MOR, even though there are ten times more frequency points. This makes sense, because in MOR analysis only two full-size eigenproblems are solved plus P full size linear matrix equations, (4.14). For the other frequency points, only the reduced eigenproblem needs to be solved, which has an almost negligible cost compared to the cost of solving a full-size eigenproblem.

Therefore, the speed up that can be achieved depends on the number of frequencies that are used in computing the dispersion diagram using the direct method. This can be seen clearly by comparing the speed up in different structures. For example, the MOR speed-up in the mushroom case is more than in the cube case (10.4 versus 7.4) because there are more frequency points used in the direct analysis of the mushroom case (111 points versus 50).

TABLE I. Comparison of the computational cost of the direct method (chapter 3) and the MOR method.

Simulated Structure		**Cube**	**Mushroom**	**LPC-EBG**	**AS-EBG**
Number of DOFs		35,500	32,232	19,968	46,530
Direct Method	Number of freq. points	50	111	61	43
	CPU Time (s)	3,027	4,140	1,756	4,287
MOR	Number of freq. points	500	1101	601	421
	CPU Time (s)	407	398	206	591
	Speed-up	7.4	10.4	8.5	7.2

Chapter 5

Adaptive Model Order Reduction

In the previous chapters, it was shown how FEM can be used for the dispersion analysis of periodic structures. Moreover it was shown that applying MOR to FE analysis reduces the computational cost significantly. One might ask what would be the motivation of continuing to work on this subject. The answer lies in addressing two very important issues.

The first issue is the eigenvalue tracking system which was introduced in chapter 3. The system was based on finding, at each frequency, the closest eigenvalue to the one obtained for the previous frequency. Although the system was shown to work very successfully in a number of cases, it has some limitations. The frequency steps have to be small enough to make sure that the right eigenmode is being tracked, but no quantative measure was given for "small enough". If it is set too big, there might an eigenvalue corresponding to a different mode that happens to be closer to the previous eigenvalue, which would cause the tracking system to switch modes. The worst case happens when the dispersion curves for two eigenmodes intersect each other.

The second issue is the limited bandwidth of the MOR method introduced in chapter 4. Looking at figures 4.1 to 4.8 in chapter 4 and comparing them with the corresponding dispersion curves in chapter 3, one sees that although the results

match very well, the MOR results are given for more limited bands of frequencies. If the bands are extended, the error grows and leads to inaccurate results. Fig. 5.1 shows how the error grows as we move away from the expansion point.

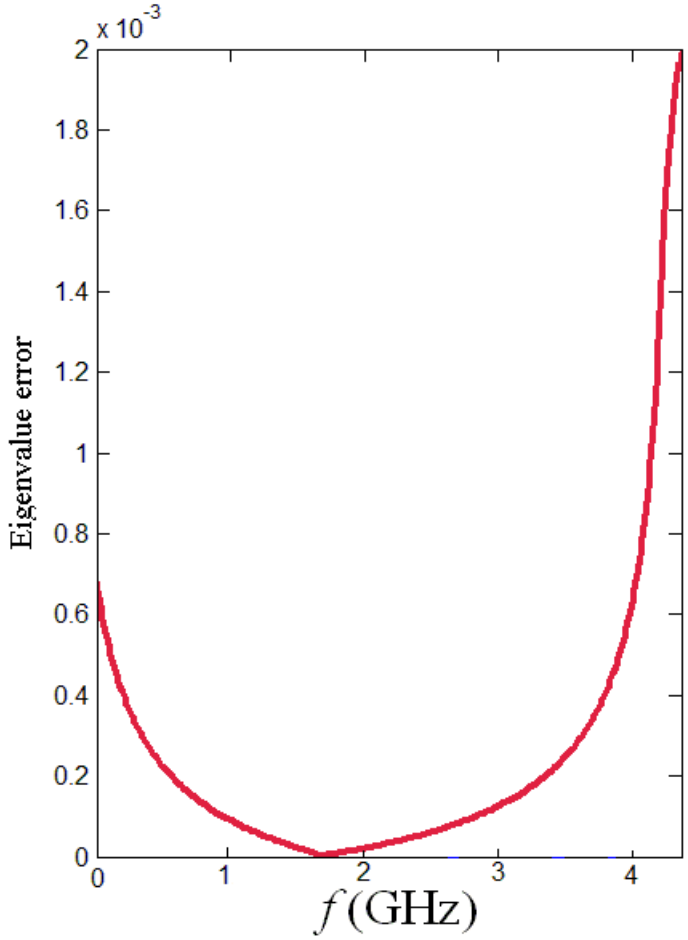

Fig. 5.1 Error in the MOR eigenvalue for the AS-EBG structure (Chapter 4, Fig. 4.8). The expansion point is at 1.8 GHz.

In this chapter both issues are addressed. A comprehensive algorithm is proposed that enables us to track any desired eigenmode over any given range of frequencies with high accuracy in a short time. The next section describes the algorithm.

5.1 Multiple expansion point MOR with adaptive tracking over a frequency range

In order to generate the dispersion curve over a given frequency range, a mechanism is required that employs new expansion points when the current expansion point stops giving results with a given accuracy. Applying this multiple expansion point mechanism requires a way of estimating the accuracy of the calculated eigenvalue at any frequency point. The details of the multiple expansion point procedure are explained in the following algorithm.

The other issue that is addressed in the algorithm is making sure that the correct eigenmode is tracked over the frequency range and that an eigenvalue belonging to another mode is not picked accidently. The automatic adjustment of the frequency step size is an important part of the tracking mechanism.

5.2 The adaptive FE-MOR algorithm

The algorithm is written in pseudocode format from the top level downwards At each level the pseudo code comes first and the corresponding interpretation follows. Bold-face indicates pseudo code that is later expanded into further pseudo code.

Initialization (5.2.1).

Repeat:

build an MOR system at a new expansion point (5.2.2);

find λ vs. k_0 using MOR until the error is too big (5.2.3);

until the desired frequency range has been covered.

5.2.1 Initialization

Select an initial step size, dk.

Solve a fixed-γ problem to get the initial point, k_{0i}.

Set $k_0 = k_{0i}$.

After selecting an arbitrary frequency step size, the algorithm requires a good guess for the eigenvalue of the starting frequency point. The best way to do so is to solve a fixed-γ problem (section 2.3.1) for a passband point like $\gamma D = j\frac{\pi}{2}$ (this is the value used for the results below). The calculated eigenvalues for this problem are different wavenumbers, each of which belongs to a different dispersion mode. The only thing that needs to be done is to select as the initial point, k_{0i}, the wavenumber corresponding to the mode of interest and the algorithm will generate the dispersion curve for that mode.

The initial step size, dk, is actually the greatest step size that will be used in the algorithm. It will be reduced automatically whenever it is necessary.

5.2.2. Build an MOR system at a new expansion point

For the first expansion point, the method described in chapter 4 is used at the

wavenumber k_0 determined by the initialization. Using the Arnoldi method, the closest eigenvalue to $C_x = e^{-\gamma D}$ is found, where γD is the value used for the initial fixed-γ problem. Then following the procedure explained in chapter 4, the $n \times L$ matrix $[E]$ is computed the $L \times L$ eigenproblem is set up and solved for all L eigenvectors.

For subsequent expansion points, the following algorithm is applied:

Let k_e *= last expansion point, with expansion matrix* $[E]$

Let λ *and* $\{y\}$ *be the eigenvalue and eigenvector of the last frequency point.*

Repeat:

Set $\{v_{old}\} = [E]\{y\}$.

Solve the $n \times n$ *eigenproblem at* k_0 *, for 2 eigenvalues closest to* λ.

Find the angle, θ*, between* $\{v_{old}\}$ *and the two eigenvectors,* $\{v_1\}$ *and* $\{v_2\}$.

If this angle is too big ($\cos\theta < 0.8$*):*

Set k_0 *= biggest frequency* $\leq \frac{k_e + k_0}{2}$ *at which* λ *and* $\{y\}$ *are available.*

If $k_0 = k_e$ *: Abort.*

Set λ *and {y} to the values obtained there.*

Until angle is small enough.

Choose the tracking eigenpair, λ**,** $\{v\}$.

Find the MOR expansion vectors for $\{v\}$.

From them, compute the $n \times L$ *matrix* $[E]$.

Solve the $L \times L$ *eigenproblem at* k_0 *, for all L eigenvectors.*

Let $\{y\}$*=eigenvector in* $[E]$ *which has eigenvalue* λ .

Since a small increment in frequency is expected to make a small change in the corresponding eigenpair $(\lambda, \{v\})$, the eigenpair at the new expansion point is established by using Arnoldi to find the eigenvalue closest to the eigenvalue at the last (i.e., closest) frequency. However it is not enough to ask Arnoldi to find just this one eigenvalue, because if the previous eigenvalue was at, or very close to, the intersection of two dispersion curves, the eigenvalue selected by this procedure could easily lie on the wrong dispersion curve. Instead, Arnoldi is asked to find both the closest and the next closest eigenvalues. Between these two eigenvalues, the one whose eigenvector creates a smaller angle with $\{v_{old}\}$ is selected as the new expansion point. This ensures that the correct dispersion mode is tracked by the algorithm and the rest of the MOR procedure is followed as explained in chapter 4.

It may happen that the two new eigenvectors are too different from $\{v_{old}\}$ for this procedure to be reliable. To check this, the angle, θ, between $\{v_{old}\}$ and the two-dimensional space spanned by the new eigenvectors, $\{v_1\}$ and $\{v_2\}$, is found, using:

$$\cos\theta = \frac{|v^H P v|}{\|v\| \|Pv\|} \tag{5.1}$$

where $[P]\{v\}$ is the orthogonal projection of $\{v\}$ onto the space spanned by

$\{v_1\}$ and $\{v_2\}$. If $\cos\theta$ is not close enough to 1, an incorrect eigenmode is being tracked by the reduced order model and the correct eigenmode has been lost somewhere between the previous expansion point and the new expansion point. In such a case, the only solution is to try to find out where the correct mode has been lost. To do that the frequency band between the new expansion point and the old one is bisected and an MOR solution close to this middle point is considered as the new expansion point. The procedure is repeated until a small enough angle is found.

To find out which of the two eigenpairs is the right one to be followed in order to calculate the rest of the dispersion curve, the following piece of pseudocode is used:

Choose the tracking eigenpair, λ***,*** $\{v\}$***.***

If either λ_1 *or* λ_2 *(but not both) has a magnitude greater than* $1+10^{-4}$*:*

Choose the other eigenvalue as tracking.

Else if either λ_1 *or* λ_2 *(but not both) is in the lower half space (Imag(*λ_i*)* $< -10^{-4}$*):*

Choose the other eigenvalue as tracking.

Else

Find the angle between $\{v_1\}$ *and* $\{v_{old}\}$.

Find the angle between $\{v_2\}$ *and* $\{v_{old}\}$.

The eigenvector with the smaller angle is tracking.

Set λ***,*** $\{v\}$ *to the tracking eigenpair.*

The first criterion that has to be tested to choose the right eigenpair is to check if the mode is physical. Any eigenvalue having a magnitude greater than 1 has to be rejected since it represents exponential growth. The second thing that is checked is whether or not the eigenvalue is located in the upper half space of the complex plane. The validity of this test lies in the fact that the eigenvalues always occur in conjugate pairs for lossless problems [56]. Therefore this is sufficient to arbitrarily choose to compute only the eigenvalues with positive or zero imaginary part.

In most cases, the eigenvalues pass both of these tests. The tie breaker then is comparing the angle that each eigenvector makes with the previous eigenvector. The one with the smaller angle is chosen.

Next the MOR procedure from chapter 4 is applied to generate the $n \times L$ matrix $[E]$. In implementing this, the value P=15 is used for all the results. Since the first column of E is just a scaled version of x_0, the reduced eigenvector y that corresponds to x_0 is just $(1,0,\ldots.,0)^T$.

5.2.3 Find λ vs. k_0 using MOR until the error is too big

Set $dk_r = dk$

Repeat

Record solution point k_0, λ.

Set flag limitReached to true if a band limit has been met.

DoOneFrequencyStep $(\boldsymbol{k_0}, \boldsymbol{dk_r}, [\boldsymbol{E}], \{\boldsymbol{y}\}, \boldsymbol{\lambda})$.

Estimate the MOR error in .

Until MOR error is greater than predetermined threshold or limitReached.

Set $\{y\}$ *and* λ *to the values for the frequency* $k_0 - dk_r$.

This is the part of algorithm that sweeps the frequency band and finds the eigenvalue at each frequency point using the reduced order model. It also detects when the expansion point needs to be replaced with a new one. The following lines show how the eigenvalue is found for each frequency point.

DoOneFrequencyStep $(\boldsymbol{k_0}, \boldsymbol{dk_r}, [\boldsymbol{E}], \{\boldsymbol{y}\}, \boldsymbol{\lambda})$.

$\{y_{old}\} = \{y\}$.

Repeat

$k_0 = k_0 + dk_r$.

Use $[E]$ *to build the reduced matrices* $[E]^H[A][E], [E]^H[B][E]$ *at* k_0.

Solve the $L \times L$ *eigenproblem at* k_0 *, for all* L *eigenvectors.*

Find eigenvector $\{y\}$ *with the smallest angle to* $\{y_{old}\}$.

If angle is greater than predetermined threshold:

Find the angle between $\{y_{old}\}$ *and each pair of eigenvectors in turn.*

Let $\{y_1\}, \{y_2\}$ *be the pair with the smallest angle.*

If angle is greater than predetermined threshold:

$k_0 = k_0 - dk_r$

$$dk_r = \frac{dk_r}{2}$$

Until angle is less than predetermined threshold

If a pair of eigenvectors was found:

Choose the tracking eigenvector, {y}.

First of all the reduced size eigenproblem ($L \times L$) is solved for all L eigenvalues and eigenvectors. Now that L eigenpairs have been calculated, a mechanism is needed to choose the correct one. This mechanism is based on the angle that the calculated eigenvectors make with the eigenvector, $\{y_{old}\}$, corresponding to the previous frequency point. The smallest angle determines the correct eigenpair, provided the smallest angle is smaller than a given tolerance. If this condition is not satisfied there might be two possibilities: either this point is close to where two dispersion curves cross or the frequency step is too big and the correct mode may have been lost. First the angle between $\{y_{old}\}$ and the space spanned by each pair of eigenvectors in turn is found. If the smallest of these angles satisfies the tolerance condition then the tracking eigenvector is chosen from those two using the procedure explained in 5.2.2. Otherwise, the step size is halved, and the reduced eigenproblem is solved again for the new point, which is closer to the previous point. This continues until the smallest angle meets the tolerance. After that the eigenvector with the smallest angle becomes the new $\{y\}$.

This procedure generates the dispersion curve gradually while the computational cost is very low. Since the step size is adjusted automatically, tracking the right mode is also guaranteed. The only thing left is to recognize when the bandwidth of the expansion point is over and the eigenvalues found for the reduced order model are not matching the ones that would have been found if the full eigenproblem were solved. This issue can be addressed by estimating the difference between the MOR eigenvalue and the “full size” eigenvalue. This error

estimator is calculated as follows:

$$e_\lambda = \|\{a\} - \{b\}\| \tag{5.2}$$

where

$$\{a\} = \frac{[A]\{x\}}{\|Bx\|} \tag{5.3}$$

and

$$\{b\} = \frac{\lambda[B]\{x\}}{\|Bx\|} \tag{5.4}$$

In equation (5.3), λ is the MOR eigenvalue and $\{x\}$ is the corresponding full-size eigenvector, which is calculated from the MOR eigenvector, $\{y\}$, using

$$\{x\} = [E]\{y\} \tag{5.5}$$

For an accurate λ and an accurate $\{x\}$ the eigenvalue equation $[A]\{x\} = \lambda[B]\{x\}$ is satisfied exactly and then e_λ is zero. In addition, we have $\|b\| = |\lambda|$. The reliability of the error estimator will be examined later, in the results section.

One might ask whether this error estimation will increase the cost of the algorithm, since the matrices $[A]$ and $[B]$ have to be built at each frequency point. The answer is that although $[A]$ and $[B]$ are expensive to build, the vectors $[A]\{x\}$ and $[B]\{x\}$ can be built cheaply from the matrices $[A_{Ep}]$ and $[B_{Ep}]$, which are $n \times L$ matrices constructed once per expansion point:

$$[A_{Ep}] = [A_p][E]$$

$$[B_{Ep}] = [B_p][E] \qquad (5.6)$$

$$\text{for } p = 0,1,2$$

The vectors $[A]\{x\}$ and $[B]\{x\}$ are then found using:

$$[A]\{x\} = \left(\sum_{p=0}^{2} [A_{Ep}](k_0 - k_e)^p\right)\{y\}$$

&

$$[B]\{x\} = \left(\sum_{p=0}^{2} [B_{Ep}](k_0 - k_e)^p\right)\{y\} \qquad (5.7)$$

Once the error estimate is greater than a given threshold, the loop is aborted and a new expansion point is inserted.

As an alternative to the above error estimator, a second error estimator was considered which has almost no cost, but might not be valid for all situations. This error estimator is based on the fact that usually the true propagation constant, γ, is either purely real or purely imaginary. If the calculated γ is neither real nor imaginary, it indicates that a new expansion point needs to be employed. Although this procedure is very cheap, it is not recommended for all structures because of its lack of generality. First of all, the assumption that the propagation constant is either purely real or purely imaginary is not proven to be correct all the time. Secondly, it might be possible that an eigenvalue passes the test and yet is not the correct eigenvalue, i.e., it is an incorrect eigenvalue which happens to be either real or imaginary. The reason that, despite the lack of the generality, this approach is mentioned is that it has given satisfactory results for all the structures that have been analyzed so far.

5.3 Results

In this section the four structures that have been analyzed in chapters 3 and 4, are analyzed again using the algorithm given above. All of the results obtained are compared with those obtained independently in the published literature. Of course for some of the structures, only the passband results are available for comparison.

In addition, a new structure is analyzed in this chapter, called corrugated waveguide. This structure is a rectangular waveguide periodically loaded with

asymmetrical capacitive irises [44]. For this structure, the dispersion curve produced by the new algorithm is compared both in the passband and stopband with the results obtained using the integral equation method in [44].

In all structures studied in this section, third order elements are used [39]. Geometric models and unstructured tetrahedral meshes, respecting the periodic constraints, were built using commercial FE software [44]. The initial step size for k_0 is 0.01 rad/m and the threshold for the eigenvalue error is 10^{-3}.

Later on in this section, the estimated error is plotted for one of the periodic structures and at the end the efficiency of the algorithm is assessed.

5.3.1 The metallic cube

The first example is the PEC cube centered in a cubic, air-filled cell. The structure is analyzed using the new algorithm and as seen in Fig. 5.2, the whole dispersion curve is calculated employing 7 expansion points, which are shown as crosses on the frequency axis in this and subsequent figures.

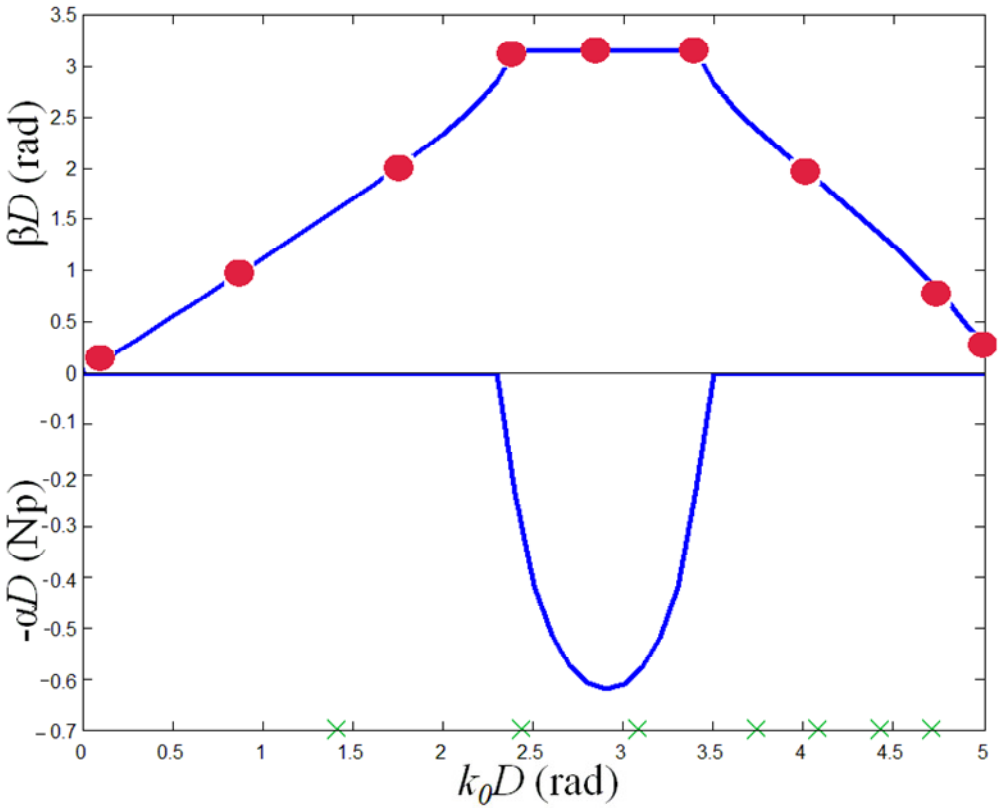

Fig. 5.2 Dispersion curve for a triply-periodic array of PEC cubes. The solid line corresponds to the results obtained with the new algorithm while the circles are from [28]. The period D is10mm. The number of tetrahedral elements is 1,925 and the matrix size is 35,500.

5.3.2 The mushroom structure

The second example is the mushroom structure: a metal square connected to the ground plane by a PEC via through the substrate. Although the structure has been described in detail in the previous chapters, a top view of the model is inset inside the dispersion diagram. As can be seen in Fig. 5.3, the frequency band of 14 GHz is handled with 4 expansion points.

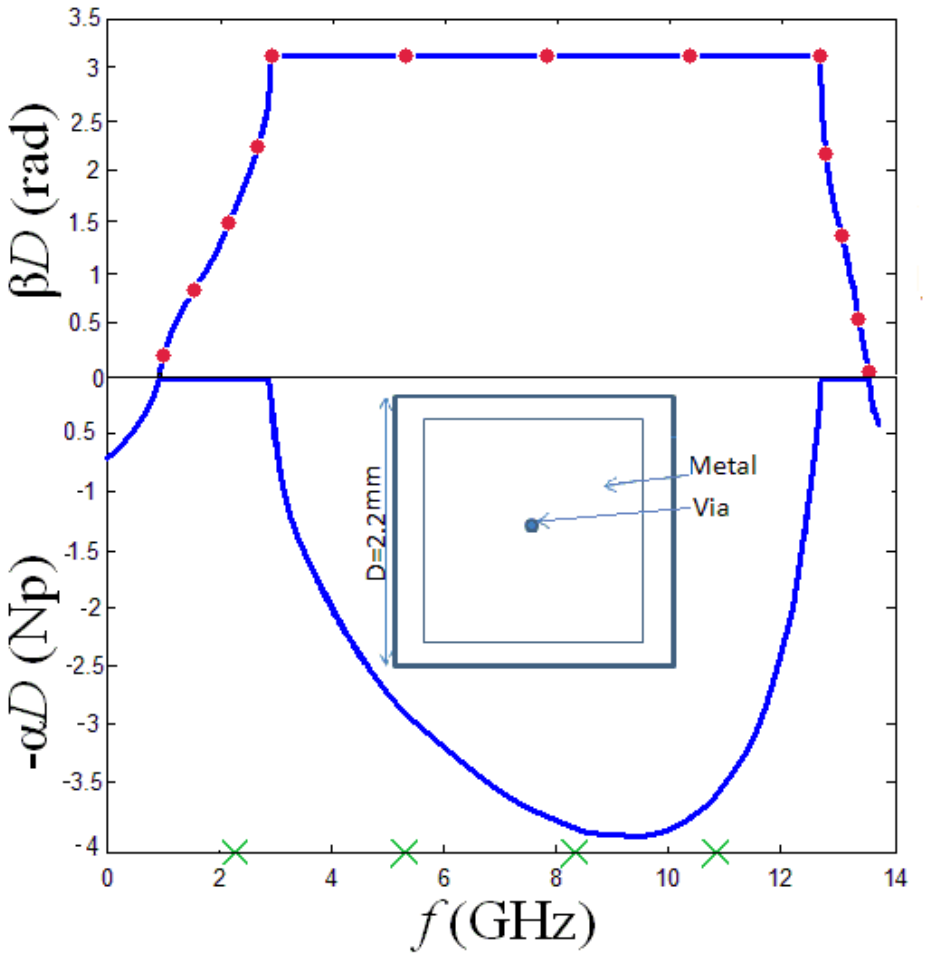

Fig. 5.3 Dispersion curve for a simple mushroom structure. The solid line corresponds to the results obtained with the new algorithm while the circles are from [9]. The period D =2.2 mm. The number of tetrahedral elements is 2,047 and the matrix size is 32,232.

5.3.3 The LPC-EBG structure

The third example is the long periodic coplanar EBG structure (LPC-EBG). Again the geometry of the structure is repeated here as an inset inside the dispersion diagram. As can be seen in Fig. 5.4, the given frequency band of 4.5

GHz needs only 2 expansion points to give the results with the required accuracy.

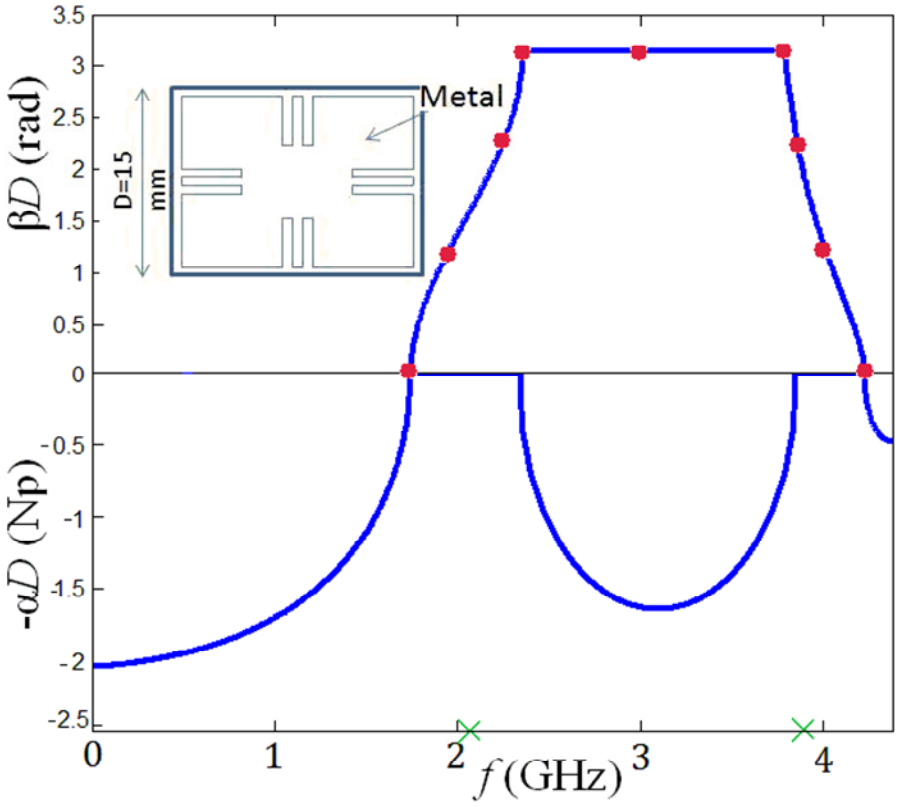

Fig. 5.4 Dispersion curve for LPC-EBG structure. The solid line corresponds to the results obtained with the new algorithm while the circles are from [40]. The period D =15 mm. The number of tetrahedral elements is 1,032 and the matrix size is 19,968.

5.3.4 The AS-EBG structure

The fourth example is the artificial substrate-EBG structure (AS-EBG). Again the geometry of the structure is repeated here as an inset inside the dispersion diagram. Fig. 5.5 shows the dispersion diagram corresponding to this structure,

which is obtained with 3 expansion points.

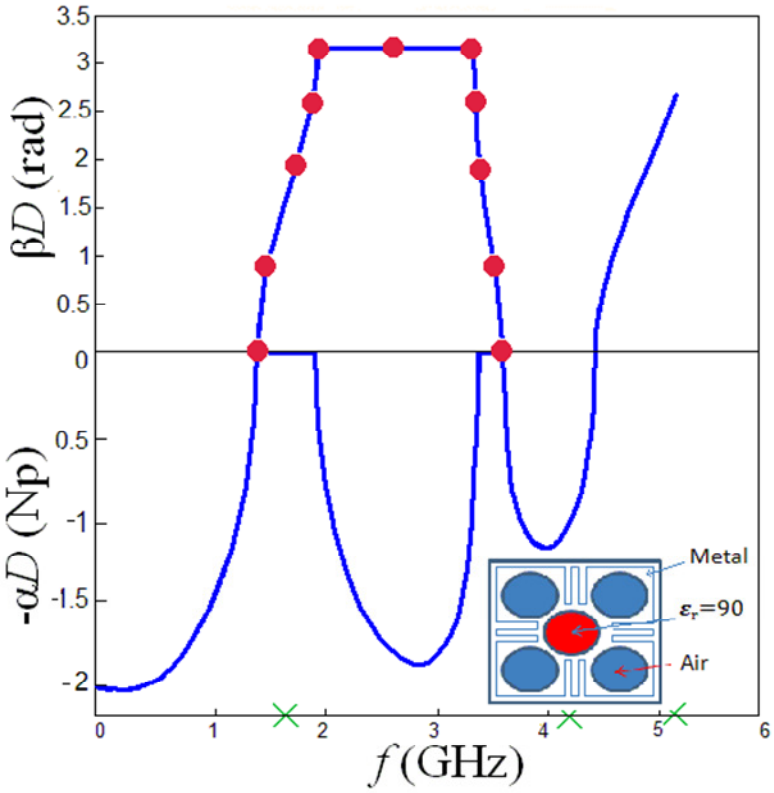

Fig. 5.5 Dispersion curve for AS-EBG structure. The solid line corresponds to the results obtained with the new algorithm while the circles are from [40]. The period D =15 mm. The number of tetrahedral elements is 2,427 and the matrix size is 46,530.

5.3.5 The corrugated waveguide

The final example is a rectangular waveguide periodically loaded with asymmetrical capacitive irises[44]. This structure is singly periodic. The rectangular waveguide is 22.86 mm x 5.08 mm in cross-section and the E-plane of one cell is shown inset in Fig. 5.6. The results are compared in both passbands and stopbands with those obtained independently, by an integral equation method [44].

Fig. 5.6 shows the dispersion diagram of this structure which is obtained with 9 expansion points.

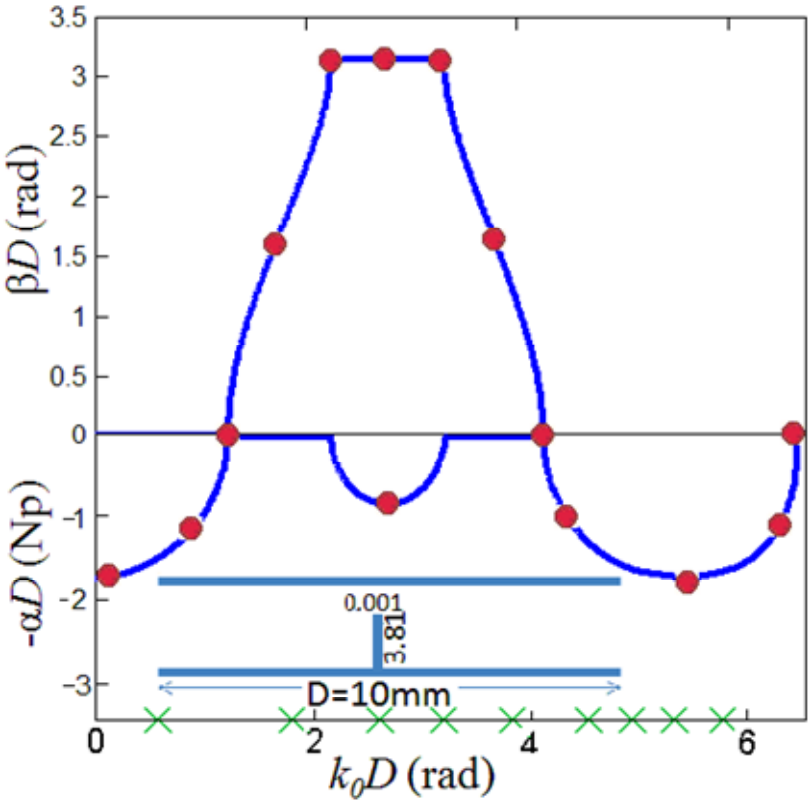

Fig. 5.6 Dispersion curve for a waveguide loaded with capacitive irises. Solid line corresponds to the results obtained with the new algorithm while the circles are from [40]. Dimensions shown are in mm. The number of tetrahedral elements is 893 and the matrix size is 20,898.

5.3.6 MOR eigenvalue error

The results presented so far demonstrate the ability of the proposed algorithm to compute eigenvalues accurately and generate the dispersion curve through both passbands and stopbands.

In all the examples the threshold for the eigenvalue error was set to 10^{-3}, which is a threshold satisfied by the estimated error and not the real error. Obtaining the real error requires solving the full eigenvalue problem at each frequency point which is very expensive. In order to examine the reliability of the error estimator, in this section the real error is calculated for the AS-EBG structure. Fig. 5.7 plots this error when the threshold is set to 10^{-3} while Fig. 5.8 plots it for a threshold of 10^{-4}. The decrease to zero error occurs at the expansion points. As expected, it can be seen that the higher accuracy requires more expansion points. The interesting point is that in both cases the error stays with a factor of 2 of the threshold value used.

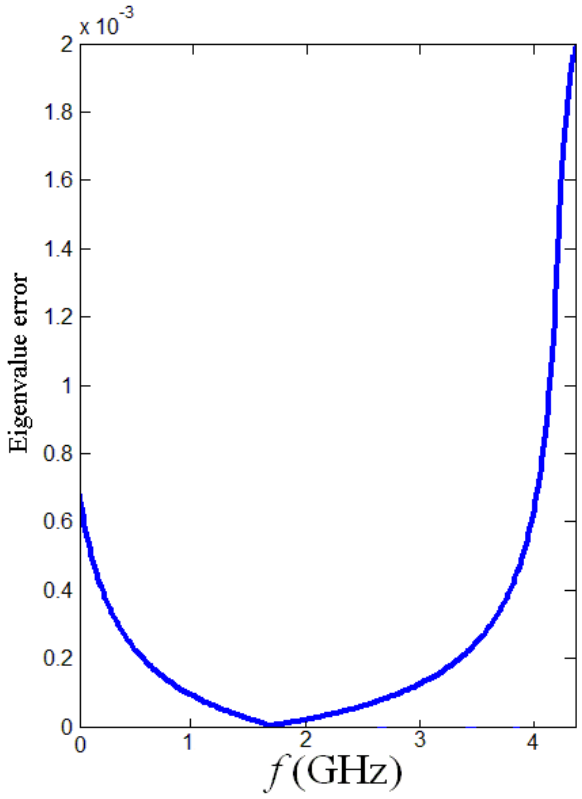

Fig. 5.7 The true eigenvalue error versus frequency when the eigenvalue error threshold is 10^{-3}

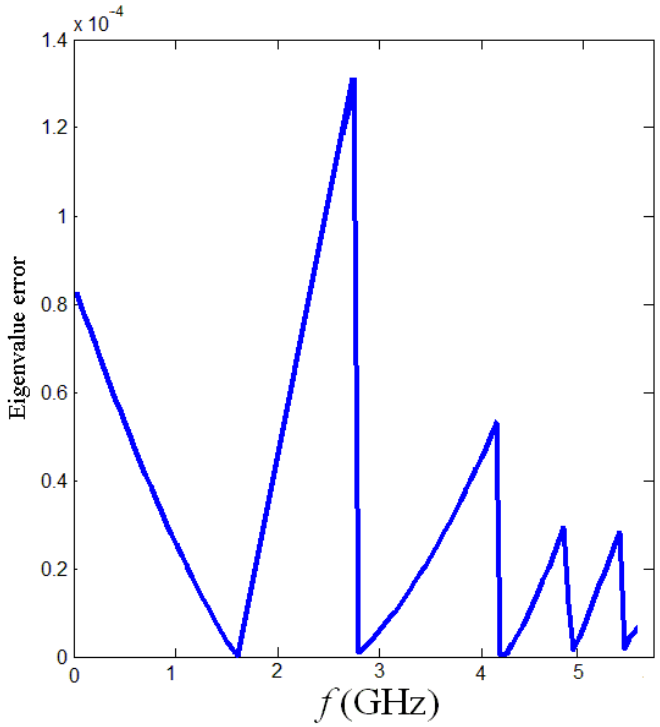

Fig. 5.8 The true eigenvalue error versus frequency when the eigenvalue error threshold is 10^{-4}

5.3.7 Computation time

This section presents the efficiency of the algorithm. In Table I, the dimensions and timings for all five test structures are given. Three different sets of times are presented. The first set gives the time for solving one full-sized eigenproblem, $[A]\{x\} = \lambda[B]\{x\}$, using the Arnoldi method to find one mode. The other two sets provide the timing information for the solution of the whole frequency band using the algorithm proposed in this chapter. The only difference between these two sets is the initial step size for k_0. The examples in this chapter have all been solved with the initial step size of 0.01 rad/m (the period D is between 2.2 mm and 15 mm for these test cases). One set represents this initial step size and the other set represents an initial step size 10 times bigger (i.e., 0.1 rad/m).

In the first case, the algorithm never needs to reduce the step size to meet the angle threshold for all examples, while in the second case there are situations where the step size is reduced by the adaptive mechanism of the algorithm. For both values of the initial step size the number of expansion points is the same and the plots are obtained with the same accuracy. There are two important points here. First of all, any value can be given to the algorithm as the initial step size and the algorithm refines it itself whenever it is needed. The second point is that there is only a small difference in the computation time, because most of the time is taken by the calculations at the expansion points.

For these problems, the direct method typically needs a step size of around 1 rad/m for reliable tracking. From the timings in the table, then, it is evident that the cost of the solution by adaptive MOR is more than 10 times less than the cost of the direct solution.

TABLE I PROBLEM SIZES AND TIMINGS

	Cube	Mush-room	LPC-EBG	AS-EBG	Loaded waveguide
Elements	1,925	2,047	1,032	2,427	893
Matrix size, n	35,500	32,232	19,968	46,530	20,828
Time (s) for solving one nxn eigenproblem	61	41	29	98	30
MOR, Initial step size=0.01 rad/m					
Number of expansion points	7	4	2	3	9
Number of frequency points	50,001	25,001	8,001	11,001	63,001
Total time (s)	2,734	929	382	1,403	1,753
MOR, Initial step size=0.1 rad/m					
Number of expansion points	7	4	2	3	9
Number of frequency points	7,442	2,957	801	1,101	8,635
Total time (s)	2,691	898	361	1,376	1,704

Chapter 6

Conclusion

6.1 Original contributions

The original contributions reported in this thesis are the following:

- Linearizing the quadratic eigenproblem resulting from fixed-k_0 finite element analysis of periodic structures, without doubling the matrix dimension.

- A model order reduction scheme for fixed-k_0 finite element analysis of periodic structures.

- A comprehensive MOR algorithm with multiple expansion points and adaptive eigenmode tracking to generate the dispersion curve of periodic structures rapidly and accurately.

6.2 Discussion

In the past few decades periodic structures have been an active and growing subject in the field of microwave electromagnetics. Periodic structures have found application in power distribution networks, filters, antennas and even in artificial materials. For designers, exploiting the merits of periodic structures requires a deep understanding of the wave dispersion in these structures. They either need to conduct a deterministic study by introducing a source and observing the scattering parameters of the structure or to conduct an eigenvalue analysis of the unit cell of the periodic structure in order to obtain the characteristic modes . Only the eigenvalue analysis can provide complete dispersion curves. Applying the conventional method of eigenvalue analysis offered by commercial software requires the designer to specify a purely imaginary Floquet propagation constant ($\gamma = j\beta$) and to seek the corresponding frequency (k_0). Plotting the so-called $k - \beta$ diagram is the result of this analysis.

Imagine that an engineer needs to investigate the insertion loss characteristics of an EBG filter. He would need to know about the evanescent modes of the periodic structure, which is not possible with the conventional method. He needs a tool that can find the evanescent and even complex modes of the structure that he is studying.

Now imagine another scenario in which the engineer is not interested in the evanescent mode. He does not even care what happens in the stopband. He simply needs to see the $k - \beta$ diagram, but the problem is that he has a material in his structure which is lossy or frequency dependant. Again he is unable to analyze that structure with the conventional method which specifies β and seeks the frequency. He needs a tool that allows him to specify the frequency and gives him the complex propagation constant at that frequency. This way he can use any kind of material in his design no matter if is lossy, anisotropic or even frequency dependant.

The suggested method in [29] is a remedy for these shortcomings. In this method the frequency (k_0) is specified and the dispersion equation is solved for

the complex γ. This way all the eigenmodes including complex modes of the structure can be found and both $k-\beta$ and $k-\alpha$ diagrams are obtained by plotting the imaginary and the real part of γ versus frequency. The only drawback of this method is the huge computational cost associated with a dense-matrix solution of the quadratic eigenvalue problem, which made it almost impossible to apply it to realistic 3D geometries. The three original contributions listed in the previous section are 3 steps towards solving the fixed-k_0 problem efficiently and accurately over a desired band of frequency, for any 3D geometry. The first contribution, explained in detail in chapter 3, turns the quadratic eigenvalue problem into a linear eigenproblem without increasing the matrix size or losing any generality. The only assumption made is that there should be no finite element which goes the whole way through the unit cell of the periodic structure. The second contribution, which was the subject of chapter 4, applies MOR to the analysis. By solving the eigenvalue problem for only one frequency and considering it as an expansion point, the propagation constant for a surrounding frequency band is found by solving a reduced order model. The computational cost for analyzing the whole band is only a little bit more than the cost of solving the eigenvalue problem for one point. The only drawback is that as we get further from the expansion point the error in the eigenvalue grows. The third contribution, described in chapter 5, applies multiple expansion points to the FE-MOR analysis. An error estimator is employed that indicates when the error exceeds a certain tolerance and a new expansion point needs to be selected. In this way, any given frequency band can be swept with a given accuracy. A smart adaptive tracking mechanism is proposed which guarantees that the same mode is tracked over the frequency range.

Although the method proposed in this thesis offers an efficient and accurate approach for dispersion analysis of periodic structures, there is always room for improvement. The following are some suggestions for future work:

- Applying the method to open periodic structures, like antenna arrays. This can probably be done by applying perfectly matched layers (PML) [34] to model the unbounded region.

- Investigating the complex eigenmodes of a periodic structure containing non-reciprocal material [57]. This material is usually ferrite which is biased by a static magnetic field and devices built with it can phase-shift, displace or absorb signals by different amounts, depending on the bias field and on the direction of propagation. Such structures give new degrees of freedom to designers to achieve the desired properties of the stopband because both periodicity resonance and ferromagnetic resonance can be employed in the design.

- Improving the adaptive multiple expansion point algorithm. It should be possible to use both the left and right-hand band of each expansion point.

- Applying the method to find higher propagating and evanescent modes. In all of the test cases, only the lowest mode has been studied. The higher modes can be obtained by choosing other eigenvalues of the fixed-γ problem which is solved to initiate the algorithm.

References

[1] G. Floquet, "Sure les equations differentielles lin_earies a coefficients periodiques," Ann. _ Ecole Norm. Sup., vol. 12, pp. 47-88, 1883.

[2] F. Bloch, "Uber die quantenmechanick der electronen in kristallgittern," Z. Physik, vol. 52, pp. 555-600, 1928.

[3] Collin, R.E. "Foundations for microwave engineering," McGraw-Hill, New York, 1992, 2nd edition.

[4] R. E. Collin, "Field theory of guided waves," New York , IEEE Press, 1991.

[5] E. W. Weisstein, "Fourier Series from MathWorld ,A Wolfram web resource," http://mathworld.wolfram.com/FourierSeries.html, 2006.

[6] G. V. Eleftheriades, A. K. Iyer, and P. C. Kremer, "Planar negative refractive index media using periodically L-C loaded transmission lines," IEEE Trans. Microw.Theory Tech., vol. 50, pp. 2702-2712, Dec 2002.

[7] F. Elek and G. V. Eleftheriades, "A two-dimensional uniplanar transmission-line metamaterial with a negative index of refraction," New Journal of Physics, vol. 7, pp. 1367-2630, Aug 2005.

[8] A. Grbic and G. V. Eleftheriades, "Periodic analysis of a 2-D negative refractive index transmission line structure," IEEE Trans. Antennas and Propagation, vol. 51, pp. 2604-2611, Oct 2003.

[9] A. Tavallaee and R. Abhari, "2-D characterisation of electromagnetic bandgap structures employed in power distribution networks," *IET Microwaves Antennas & Propagation*, vol. 1, pp. 204-211, Feb 2007.

[10] A. K. Iyer and G. V. Eleftheriades, "Negative refractive index metamaterials supporting 2-D waves," IEEE MTT-S International Microwave Symposium Digest, vol. 2, pp. 1067-1070, 2-7 June 2002.

[11] C. Caloz and T. Itoh, "Transmission line approach of left-handed (LH) materials

and microstrip implementation of an artificial LH transmission line," IEEE Trans. Antennas and Propagation, vol. 52, pp. 1159-1166, May 2004.

[12] L. Brillouin, "Wave propagation in periodic structures : electric filters and crystal Lattices," New York , Dover Publications, 2nd ed., 1953.

[13]] R. Mittra, C. H. Chan, and T. Cwik, "Techniques for analyzing frequency selective surfaces-a review," Proceedings of the IEEE, vol. 76, pp. 1593-1615, Dec 1988.

[14] Da-Zhi Ding, Edward Kai-Ning Yung, and Dao-Xiang Wang and Ru-Shan Chen, "Efficient Analysis of Periodic Structures with Arbitrary Shape Using Volume-surface Integral Equation Method," Progress In Electromagnetics Research Symposium 2005, Hangzhou, China, August 22-26

[15] Rao, S. M., D. R. Wilton and A. W. Glisson, "Electromagnetic Scattering by Surfaces of Arbitrary Shape," IEEE Trans. Antennas Propagat., Vol. 32, 409-418, 1982.

[16] Kipp, R. A. and C. H. Chan, "A Numerical Efficient Technique for the Method of Moments Solution to Planar Periodic Structures in a Layered Media," IEEE Trans. Microwave Theory Tech., Vol. 42, 635-643, 1994.

[17] Wang, J. J. H., "Generalized Moment Methods in Electromagnetics," John Wiley & Sons, Inc., 1991.

[18] K. S. Yee, "Numerical solution of initial boundary value problems involving Maxwell's equations in isotropic media," IEEE Trans. Antennas and Propagation, vol. 14, pp. 302-307, May 1966.

[19] D. Prescott and N. Shuley, "Extensions to the FDTD method for the analysis of Indefinitely periodic arrays," IEEE Microwave Guided Wave Lett, vol. 4, pp. 352-354, Oct 1994.

[20] Y. Kao and R. Atkins, "A finite difference-time domain approach for frequency selective surfaces at oblique incidence," IEEE Antennas and Propagation Society International Symposium, pp. 1432-1435, 1996.

[21] J. Roden, S. Gedney, M. Kessler, J. Maloney, and P. Harms, "Time-domain analysis of periodic structures at oblique incidence: Orthogonal and nonorthogonal FDTD implementations," IEEE Trans. Microw. Theory Tech., vol. 46, pp. 420-427, Apr 1998.

[22] P. Harms, R. Mittra, and W. KO, "Implementation of the periodic boundary condition in the finite-difference time-domain algorithm for FSS

structures," IEEE Trans. Antennas and Propagation, vol. 42, pp. 1317-1324, Sept 1994.

[23] R. L. Ferrari, "Finite element solution of time-harmonic modal fields in periodic structures," Electronics Letters, vol. 27, pp. 33-34, Jan 1991.

[24] P. Olszewski, "Expansion of periodic boundary condition for 3-D FEM analysis using edge elements," IEEE Trans. Magnetics, vol. 28, pp. 1084-1087, Mar 1992.

[25] D. T. McGrath and V. P. Pyati, "Periodic boundary conditions for finite element analysis of infinite phased array antennas," IEEE Antennas and Propagation Society International Symposium, vol. 3, pp. 1502-1505, June 1994.

[26] C. Mias and R. L. Ferrari, "Closed singly periodic three dimensional waveguide analysis using vector finite elements," Electronics Letters, vol. 30, pp. 1863-1865, Oct 1994.

[27] A. Freni, C. Mias, and R. L. Ferrari, "Finite element analysis of electromagnetic plane wave scattering from axially periodic cylindrical structures," IEEE Antennas and Propagation Society International Symposium, vol. 1, pp. 146-149, July 1996.

[28] C. Mias, J. P. Webb, and R. L. Ferrari, "Finite element modeling of electromagnetic waves in doubly and triply periodic structures," IEE Proc. Optoelectronics, vol. 146, pp. 111-118, April 1999.

[29] A. Tavallaee and J. P. Webb, "Finite-element modeling of evanescent modes in the stopband of periodic structures," *IEEE Transactions on Magnetics*, vol. 44, no. 6, pp.1358–1361, June 2008.

[30] M. Davanco, Y. Urzhumov, and G. Shvets, "The complex Bloch bands of a 2D plasmonic crystal displaying isotropic negative refraction," *Optics Express*, vol. 15, pp. 9681-9691, Jul 23 2007.

[31] A. Bostani and J. P. Webb, "A Sparse Finite-Element Method for Modeling Evanescent Modes in the Stopband of Periodic Structures," *IEEE Trans. on Magnetics,* vol. 47, pp. 1186-1189, May 2011.

[32] A. Bostani, J. P. Webb, "A model-order reduction method for the passband and stopband characteristics of periodic structures", *41st European Microwave Conference Proceedings*, Manchester, UK, October 10-13, 2011.

[33] S. Guo and S. Albin, "Simple plane wave implementation for photonic crystal calculations," Optics Express, vol. 11, pp. 167-175, 2003.

[34] J. Jin, "The Finite Elements Method in Electromagnetics." New York: Wiley, 2nd ed., 2002.

[35] C. B. Moler and G. W. Stewart, "An algorithm for generalized matrix eigenvalue
problems," SIAM J. Num. Anal., vol. 10, pp. 241-256, May 1973.

[36] V. N. Kublanovskaya, "On an approach to the solution of the generalized latent value problem for _-matrices," SIAM J. Num. Anal., vol. 7, 1970.

[37] A. Ruhe, "Algorithms for the nonlinear eigenvalue problem," SIAM J. Num. Anal., vol. 10, pp. 674-689, Sept 1973.

[38] A. Nicolet, S. Guenneau, C. Geuzaine, and F. Zolla, "Modeling of electromagnetic waves in periodic media with finite elements," *Journal of Computational and Applied Mathematics*, vol. 168, pp. 321-329, Jul 1 2004.

[39] J. P. Webb, "Hierarchal vector basis functions of arbitrary order for triangular and tetrahedral finite elements", *IEEE Trans. Antennas Propag.*, vol. 47, no. 8, pp. 1244 - 1253, 1999.

[40] Ting-Kuang Wang, Tzu-Wei Han, Tzong-Lin Wu, "A Novel Power/Ground Layer Using Artificial Substrate EBG for Simultaneously Switching Noise Suppression," *IEEE Trans. on Microwave Theory and Techniques,* vol.56, no.5, pp.1164-1171, May 2008.

[41] S. H. Lee, T. Y. Huang, and R. B. Wu, "Fast waveguide eigenanalysis by wide-band finite-element model-order reduction," *IEEE Transactions on Microwave Theory and Techniques*, vol. 53, pp. 2552-2558, Aug 2005.

[42] F. Bertazzi, O. A. Peverini, M. Goano, G. Ghione, R. Orta, and R. Tascone, "A fast reduced-order model for the full-wave FEM analysis of lossy inhomogeneous anisotropic waveguides," *IEEE Transactions on Microwave Theory and Techniques,* vol. 50, pp. 2108-2114, Sep 2002.

[43] C. Scheiber, A. Schultschik, O. Bíró, R. Dyczij-Edlinger, "A model order reduction method for efficient band structure calculations of photonic crystals," *Electromagnetic Field Computation (CEFC), 2010 14th Biennial IEEE Conference on* , vol., no., pp.1, 9-12 May 2010.

[44] S. Marini, A. Coves, V. E. Boria, and B. Gimeno, "Efficient Modal Analysis of Periodic Structures Loaded With Arbitrarily Shaped Waveguides,"

IEEE Trans. on Microwave Theory and Techniques, vol. 58, pp. 529-536, Mar 2010.

[45] P. Baccarelli, C. Di Nallo, S. Paulotto, D.R. Jackson , "A full-wave numerical approach for modal analysis of 1-D periodic microstrip structures," *Microwave Theory and Techniques, IEEE Transactions on* , vol.54, no.4, pp. 1350- 1362, June 2006.

[46] P. Baccarelli, S. Paulotto, C. Di Nallo, "Modal Analysis of Arbitrary-shaped 2D Periodic Structures Printed on a Grounded Dielectric Slab: Real and Complex Solutions,"*Microwave Symposium Digest, 2006. IEEE MTT-S International* , vol., no., pp.1465-1468, 11-16 June 2006.

[47] F. Xu, and W. Hong, "A Novel FDFD Method for the Electromagnetic Analysis of Guided Waves in Periodic Structures," CJMW'2002, pp.129-132, Apr. 2002.

[48] F. Xu, Y. Zhang, W. Hong, K. Wu and T. J. Cui, "Finitedifference frequency-domain algorithm for modeling guided-wave properties of substrate integrated waveguide," IEEE Trans. Microwave Theory Tech., vol. 51, no. 11, pp.2221-2227, November, 2003.

[49] Feng Xu , Ke Wu , "Application of the Arnoldi method in FDFD analysis of periodic guided-wave structure," *Microwave Conference, 2005 European* , vol.2, no., pp. 4 pp., 4-6 Oct. 2005

[50] Webb, J.P., "Edge elements and what they can do for you," *Magnetics, IEEE Transactions on* , vol.29, no.2, pp.1460-1465, Mar 1993

[51] HFSS, ANSYS Corporation. http://www.ansys.com/Products/Simulation+Technology/Electromagnetics/High-Performance+Electronic+Design/ANSYS+HFSS

[52] Saad, Yousef. "Iterative Methods for Sparse Linear Systems." Ed. Siam. *IEEE Computational Science and Engineering* 3.4 (1996).

[53] Obinata, G. And Anderson, B.D.O., "Model reduction for control system design," , Springer-Velag, London, 2001.

[54] Arif, Mohammad; Anand, R. S. , "Application of model order reduction approach on quality evaluation of speech signal," *Computational Intelligence and Signal Processing (CISP), 2012 2nd National Conference on* , vol., no., pp.136-140, 2-3 March 2012.

[55] Dautbegovic, E. Condon, M.; Brennan, C. , "An efficient wavelet-based nonlinear circuit simulation technique with model order reduction," *High Frequency Postgraduate Student Colloquium, 2004* , vol., no., pp. 119- 124, 6-7 Sept. 2004

[56] Carl D. Mayer "Matrix analysis and applied linear algebra," Society for Industrial and Applied Mathematics Philadelphia, PA, USA ©2000, ISBN:0-89871-454-0 .

[57] O. V. Shramkova, "Transmission spectra in ferrite-semiconductor periodic structure," *Progress In Electromagnetics Research M*, Vol. 7, 71-85, 2009.

[58] A. Bostani and J. P. Webb, "Finite Element Eigenvalue Analysis of Propagating and Evanescent Modes in 3D Periodic Structures using Model Order Reduction", IEEE Transactions on Microwave theory and Technique, Accepted.